

ISSN: 2164-5388 Volume 11, Number 4, October 2021



Open Journal of Biophysics

BIOPHYSICS

ISSN: 2164-5388



9 772164 153802 04

<https://www.scirp.org/journal/ojbiphy>

Journal Editorial Board

ISSN Print: 2164-5388 ISSN Online: 2164-5396

<https://www.scirp.org/journal/ojbiph>

Editor-in-Chief

Prof. W. John Martin

Institute of Progressive Medicine, USA

Associate Editors

Dr. Veysel Kayser

Massachusetts Institute of Technology, USA

Prof. Ganhui Lan

George Washington University, USA

Dr. Jaan Männik

University of Tennessee, USA

Prof. Sanbo Qin

Florida State University, USA

Dr. Bo Sun

Oregon State University, USA

Dr. Bin Tang

South University of Science and Technology of China, China

Editorial Board

Prof. Rabiul Ahasan

University of Oulu, Finland

Prof. Abass Alavi

University of Pennsylvania, USA

Prof. Chris Bystroff

Rensselaer Polytechnic Institute, USA

Dr. Luigi Maxmilian Caligiuri

University of Calabria, Italy

Prof. Robert H. Chow

University of Southern California, USA

Prof. Carmen Domene

University of Oxford, UK

Prof. Antonio José da Costa Filho

University of São Paulo, Brazil

Prof. Ferdinand Gasparyan

Yerevan State University, Armenia

Dr. John Kolega

State University of New York, USA

Prof. Pavel Kraikivski

Virginia Polytechnic Institute and State University, USA

Dr. Gee A. Lau

University of Illinois at Urbana-Champaign, USA

Prof. Yves Mély

Louis Pasteur University, France

Dr. Monalisa Mukherjea

University of Pennsylvania, USA

Dr. Xiaodong Pang

Florida State University, USA

Prof. Arthur D. Rosen

Indiana University, USA

Prof. Brian Matthew Salzberg

University of Pennsylvania, USA

Prof. Jianwei Shuai

Xiamen University, China

Prof. Mateus Webba da Silva

University of Ulster, UK

Prof. Alexander A. Spector

Johns Hopkins University, USA

Prof. Munekazu Yamakuchi

University of Rochester, USA

Table of Contents

Volume 11 Number 4

October 2021

Allometric Scaling by the Length of the Circulatory Network

A. Szasz.....359

The Possible Involvement of Apoptotic Decay of Terminal Deoxynucleotidyl Transferase-Positive Lymphocytes in the Reutilization of the Extracellular DNA Fragments by Surrounding Living Cells

A. N. Shoutko.....371

The Mystery on the Physical Conditions for Life

K. W. Wong, W. K. Chow.....383

Inventory of Radiation Protection in Hospitals of Level III in Senegal

B. Ndong, S. A. Dia, M. S. Djigo, H. Fachinan, E. H. L. Bathily, O. Diop, K. Ka, G. L. K. Akpo, E. H. F. Diouf,
L. A. D. Diouf, P. M. Sy, A. Djiboune, G. Mbaye, M. Diagne, O. Ndoye, M. Mbodji.....397

ROC and SAT Analysis of Different Grayscale Test Images (Distractors L and Target T) to Customize a Visual-Search Attention Task

D. Chuckravanen, B. Ilhan, N. Dalkılıç.....407

Novel Method Employing Accelerated-Oscillated Wave Saline Solutions to Unblock Blood Vessels—Physics and Fluid Dynamics Perspectives and Simulations

S. Stewart, D. Chuckravanen.....415

Open Journal of Biophysics (OJBIPHY)

Journal Information

SUBSCRIPTIONS

The *Open Journal of Biophysics* (Online at Scientific Research Publishing, <https://www.scirp.org/>) is published quarterly by Scientific Research Publishing, Inc., USA.

Subscription rates:

Print: \$79 per issue.

To subscribe, please contact Journals Subscriptions Department, E-mail: sub@scirp.org

SERVICES

Advertisements

Advertisement Sales Department, E-mail: service@scirp.org

Reprints (minimum quantity 100 copies)

Reprints Co-ordinator, Scientific Research Publishing, Inc., USA.

E-mail: sub@scirp.org

COPYRIGHT

Copyright and reuse rights for the front matter of the journal:

Copyright © 2021 by Scientific Research Publishing Inc.

This work is licensed under the Creative Commons Attribution International License (CC BY).

<http://creativecommons.org/licenses/by/4.0/>

Copyright for individual papers of the journal:

Copyright © 2021 by author(s) and Scientific Research Publishing Inc.

Reuse rights for individual papers:

Note: At SCIRP authors can choose between CC BY and CC BY-NC. Please consult each paper for its reuse rights.

Disclaimer of liability

Statements and opinions expressed in the articles and communications are those of the individual contributors and not the statements and opinion of Scientific Research Publishing, Inc. We assume no responsibility or liability for any damage or injury to persons or property arising out of the use of any materials, instructions, methods or ideas contained herein. We expressly disclaim any implied warranties of merchantability or fitness for a particular purpose. If expert assistance is required, the services of a competent professional person should be sought.

PRODUCTION INFORMATION

For manuscripts that have been accepted for publication, please contact:

E-mail: ojbiphy@scirp.org

Allometric Scaling by the Length of the Circulatory Network

Andras Szasz

Department of Biotechnics, St. Istvan University, Godollo, Hungary

Email: biotech@gek.szie.hu

How to cite this paper: Szasz, A. (2021) Allometric Scaling by the Length of the Circulatory Network. *Open Journal of Biophysics*, 11, 359-370.

<https://doi.org/10.4236/ojbiphy.2021.114013>

Received: June 3, 2021

Accepted: August 6, 2021

Published: August 9, 2021

Copyright © 2021 by author(s) and Scientific Research Publishing Inc.

This work is licensed under the Creative Commons Attribution International License (CC BY 4.0).

<http://creativecommons.org/licenses/by/4.0/>



Open Access

Abstract

Background: Allometric scaling is a well-known research tool used for the metabolic rates of organisms. It measures the living systems with fractal physiology. The metabolic rate versus the mass of the living species has a definite scaling and behaves like a four-dimensional phenomenon. The extended investigations focus on the mass-dependence of the various physiological parameters. **Objective:** Proving the length of vascularization is the scaling parameter instead of mass in allometric relation. **Method:** The description of the energy balance of the ontogenic growth of the tumor is an extended cell-death parameter for studying the mass balance at the cellular level. **Results:** It is shown that when a malignant cellular cluster tries to maximize its metabolic rate, it changes its allometric scaling exponent. A growth description could follow the heterogenic development of the tumor. The mass in the allometric scaling could be replaced by the average length of the circulatory system in each case. **Conclusion:** According to this concept, the dependence of the mass in allometric scaling is replaced with a more fundamental parameter, the length character of the circulatory system. The introduced scaling parameter has primary importance in cancer development, where the elongation of the circulatory length by angiogenesis is in significant demand.

Keywords

Allometry, Metabolism, Four-Dimension, Optimization, Cancer, Circulatory System, Characteristic Length

1. Introduction

The spatiotemporal organization of biosystems is complex. The complexity is driven by self-organization ([1] [2] [3]), and validated by new science: fractal physiology ([4] [5]), including the bioscaling processes ([6] [7]). Understanding

the challenges of the complexity of human medicine requires the development of a new paradigm [8].

The Basal Metabolic Rate (BMR) shows allometric scaling of the mass of the organism [9], describes as the power function of the mass (\mathcal{M}) [10]:

$$BMR \propto \mathcal{M}^\alpha \quad (1)$$

The allometric relation connects the surface-controlled metabolic processes with the geometry of the given material, which uses the available energy. In the simple formulation, metabolic processes are surface-dependent, while the mass is proportional to the volume. Therefore, the exponent of their ratio mirrors the dimensionality, and consequently, the exponent is $\alpha = 2/3$. On the other hand, the complex living allometry shows the exponent as $\alpha = 3/4$ instead of $\alpha = 2/3$ [11], explaining the relationship between the three-dimensional surface and the four-dimensional volume. Metabolic scaling in solid tumors is significant, but its heterogeneity and its rapid development by intensive proliferation and the supporting vascularity [12] change the scaling behavior [13], and this is described as dynamic evolution [14].

Life in this context is “four-dimensional” based on its metabolic exchange processes [15]. The self-organized multicellular structure creates fractal arrangements, and their metabolic energy-exchange proceeds on fractal surfaces, maximizing the available energy-consumption, scaling the fluctuation of the metabolic power by the universal scaling law [16]. This optimization of energy consumption was rigorously tested in the context of the scaling idea and can be extended to broader mechanisms [17], such as the energy-consumption's subcellular level, including the mitochondria and respiratory complexes [17].

The scaling model has been shown to be valid in a broad category of living structures and processes. The primary physiological parameters exponentially depend on the mass of the body [18]. The allometry shows a structural, geometrical constraint for living organisms. Nevertheless, life is more complex than what can be determined by its geometrical structure. A self-similar spatial-temporal-fractal structure defines the self-organizing procedure both in space and time [19]. A particular noise (temporal fractal noise)—like a fingerprint of the self-organizing [20]—is a typical and general behavior of the living biomaterial [21]. The stochastic fluctuations have a characteristic effect on malignant development [22], acting in the apoptotic threshold of cancer [23], and is well observable in the growth process [24].

The measured structural patterns could be applied to evaluate the cancer development [25] [26], an example of this is the use of image analysis is done by a pathologist. The metabolic power not only depends on the size of the surface involved in active transport, but also on the flow-rate of the same active surface size. This dependence could modify the transport. In the case of Benthic invertebrates ($n = 215$), they have the lowest average scaling exponent because they metabolize in an anaerobic way. This can be written as: ($\alpha_{mean} = 0.63$, [near to $2/3$], $CI_{mean} = 0.18$), where α is the scaling exponent, and CI is the Confidence

Interval [27]. However, the other studied animals ($n = 496$) have ($\alpha_{mean} = 0.74$, [near to $\alpha_{mean} = 3/4$], $CI_{mean} = 0.18$) [28]. The scaling of the metabolic activity is also different in mitochondrial and non-mitochondrial processes [29]. Mitochondrial metabolism is always aerobic, and its scaling exponent is nearly $\alpha = 3/4$ [30] [31]. When the oxygen supply is limited, the cell extends its ATP production to fermentation by non-mitochondrial respiration, where the allometric scaling exponent lowers to nearly $\alpha = 2/3$.

Based on the scaling theory, a general model for ontogenic growth has been proposed [32] [33] [34]. Allometry is a consequence of the evolution process [35]. The variation of the personal sizes of the organs and the whole body of the individuals can be addressed in the frame of the power-law. The high fractal dimension could be used as a significant prognostic factor in diseased tissues [36]. There is research on tumor growth evaluated from an ontogenic basis [14] [37] [38] in which the tumor is successfully described, despite the substantial heterogeneity of the blood-supply [39] and the cellular structures differing from their regular counterparts. If the whole tumor mass differs from the mass of the viable part of the tumor, and the viable part has a scaling by the complete tumor mass with a high confidence scaling exponent $\alpha = 0.78$ then the inadequate metabolic supply causes an extension of the necrotic tissue inside advanced tumors [40].

2. Method

The general model for ontogenic growth described tumor-cell growth needs to calculate the cell-production considering also the vanished cells in the energy balance [40]. We learned, however, how vital programmed cell-death (apoptosis) is in the development of the fetus of mammals [41], and we considered it as a basic biological phenomenon [42]. The concept of cell-death is crucial in cancer development, considering one of the hallmarks of the malignancy is its escape from apoptosis [43], and is instead more susceptible to a more drastic kind of death: necrosis [44]. Following the line and extensive discussion of numerous other authors [28] [30] [32] [33] [34], who adapted the death-free energy balance from the original [45] publication, we extended this view with the changes caused by the perished cells. This approach became even more relevant with the study of malignancies, where a large mass of the tumor could well involve non-living necrotic tissue, so the ontogenic calculations [37] [40] need modification based on their energy-balance.

The number of cancerous cells (N_c) is the difference between the newly produced cells (P), and the perished (due to apoptosis or necrosis) drop off cells (D) at the unit time, basically follow the method of [40]:

$$\frac{dN_c}{dt} = P - D \quad (2)$$

The value of the changing cells is zero, while production just equal to the perished cells ($P = D$). It is a realistic assumption that the perished cells are pro-

portional to the complete cell number in unit time:

$$D = \lambda N_c \quad (3)$$

where λ is the cell death-rate in a tumor. Note, at the beginning of the tumor-growth the P is also proportional with N_c , ($P = \xi N_c$) and in this case, the tumor growth exponentially: $N_{c(0)}(t) = \exp(\xi - \lambda)t$. When P is constant during the development, the balance of the cell number by the time:

$$\frac{dN_c}{dt} = P - \lambda N_c \quad (4)$$

The $P = \text{const}$ deviates from the assumption of [40]. Our consideration concentrates on the fact that the cellular production after the initial period of growth became constant due to the stabilized balance of the resources and the autonomic growth of cells in a supporting healthy host environment by resources. The situation in this phase is well similar to the *in-vitro* experiments of the monoculture system when the allometric exponent is zero [31]. The energy balance is determined by the transported energy-flux delivered by the bloodstream. The energy-transport current intensity, the metabolic rate (B), is divided into two parts: one produces new cells, while the other keeps the living set alive. Hence:

$$\begin{aligned} B &= N_c B_c + E_c P = N_c B_c + E_c \left(\frac{dN_c}{dt} + \lambda N_c \right) \\ &= N_c B_c + E_c \left(\frac{dN_c}{dt} + \frac{N_c}{T_c} \right) \end{aligned} \quad (5)$$

where B_c is the metabolic rate of a cell, and E_c is the necessary metabolic energy to create a new cell and $\lambda^{-1} = T_c$ is the average lifespan of a cell in the tumor. Consequently:

$$E_c \frac{dN_c}{dt} = B - N_c (B_c + \lambda E_c) \quad (6)$$

Metabolic energy can be scaled by exponent α ,

$$B = B_0 N_c^\alpha \quad (7)$$

where B_0 is a normalizing factor that shows the metabolic rate in the unity of N_c . Therefore, we obtain:

$$E_c \frac{dN_c}{dt} = B_0 N_c^\alpha - N_c (B_c + \lambda E_c) \quad (8)$$

Hence:

$$\begin{aligned} \frac{dN_c}{dt} &= a_c N_c^\alpha - b_c N_c \\ a_c &= \frac{B_0}{E_c}; \quad b_c = \frac{B_c}{E_c} + \lambda \end{aligned} \quad (9)$$

By multiplying N_c by the average mass of a single cell (m_c) we now obtain the energy-balance for the full tumor-mass (m):

$$\frac{dm}{dt} = am^\alpha - bm \quad (10)$$

where:

$$a = \frac{B_0 m_c^{1-\alpha}}{E_c} \quad \text{and} \quad b = \frac{B_c}{E_c} + \lambda = \frac{B_c}{E_c} + \frac{1}{T_c} \quad (11)$$

This balance was previously similarly formulated [46]. The mass has a maximum limit M , asymptotic value, a saturation when no more real changes of the mass can be observed, so:

$$0 = \frac{dM}{dt} = aM^\alpha - bM \quad (12)$$

Consequently:

$$M = \left(\frac{a}{b}\right)^{\frac{1}{1-\alpha}} = \left(\frac{B_0 m_c^{1-\alpha}}{B_c + \lambda E_c}\right)^{\frac{1}{1-\alpha}} \quad (13)$$

3. Results

A death parameter of the single-cell characteristically appears in the energy-balance of the ontogenic growth of the tumor. The nutrients supply profoundly determines the death of cancer-cells. At least at larger tumor sizes, the cell growth never happens with optimal nutrition supply; the cells intensively compete for the available energy sources.

The exponent α is located in the interval $2/3 \leq \alpha \leq 1$, and it is $\alpha = 3/4$ at ideal basal conditions [15] [45]. The ideal nutrition supply supports ontogenic growth. The “ideal” asymptotic mass (M_{id}) from (13) is: $M_{id} = \left(\frac{a}{b}\right)^{\frac{1}{1-\alpha}}$, hence the BMR^* in non-ideal conditions:

$$M = \left(\frac{a}{b}\right)^{\frac{1}{1-\alpha}} = (M_{id})^{\frac{1}{4(1-\alpha)}} \Rightarrow BMR^* = M^\alpha = (M_{id})^{\frac{\alpha}{4(1-\alpha)}} \quad (14)$$

Substituting (14) into (10):

$$\frac{dm}{dt} = am^\alpha \left(1 - \left(\frac{m}{M}\right)^{1-\alpha}\right) \quad (15)$$

So:

$$\frac{d\left(\frac{m}{M}\right)^{1-\alpha}}{dt} = \frac{a(1-\alpha)}{M^{1-\alpha}} \left(1 - \left(\frac{m}{M}\right)^{1-\alpha}\right) \quad (16)$$

which has a sigmoidal solution:

$$\begin{aligned} \left(\frac{m}{M}\right)^{1-\alpha} &= 1 - \left(1 - \left(\frac{m_0}{M}\right)^{1-\alpha}\right) e^{-\frac{a(1-\alpha)t}{M^{1-\alpha}}} \\ &= 1 - \exp\left(-\frac{at(1-\alpha)}{M^{1-\alpha}} + \ln\left(1 - \left(\frac{m_0}{M}\right)^{1-\alpha}\right)\right) \\ &= 1 - e^{-\tau} \end{aligned} \quad (17)$$

where

$$\tau = \frac{at(1-\alpha)}{M^{1-\alpha}} - \ln \left(1 - \left(\frac{m_0}{M} \right)^{1-\alpha} \right) \quad (18)$$

and m_0 is the mass at the start of a tumor (probably a few times m_c), the initial (just born) mass. The ratio (r) of the energy spent on keeping cells alive ($\lambda = 0$) from (13) is:

$$r(\tau) = \frac{N_c B_c}{B} = \frac{B_c m}{m_c B_0 m^\alpha} = \frac{b}{a} m^{1-\alpha} = \left(\frac{m}{M} \right)^{1-\alpha} = 1 - e^{-\tau} \quad (19)$$

Using $\alpha = 3/4$ for the ideal four-dimensional case, the solution is:

$$\left(\frac{m}{M} \right)^{1/4} = 1 - e^{-\tau}, \quad \tau = \frac{at}{4M^{3/4}} - \ln \left(1 - \left(\frac{m_0}{M} \right)^{1/4} \right) \quad (20)$$

This is formally the universal growth law [45], but has a difference in the values of b (see (11)) and M (see (13)), including the average life-time of the malignant cells (death rate λ) in ontology description. The M value became smaller by shortening the average life-time of the cells and elongating τ time approaching the saturatin of the mass.

4. Discussion

The four-dimensionality and the allometry with evolutionary optimization require different approaches: as the evolutionary conditions have a higher than a four-dimensional allometric scaling. The tumor mass is a somewhat indefinite parameter because the whole environment of the tumor suffers from sub-optimal alimentation. Consequently, the mass does not describe the allometry well. A more fundamental parameter of the networking conditions is requested.

From the original “four-dimensional life” fractal concept, we get scaling of the characteristic volume (v) with a characteristic length (l) [15] [45]:

$$v = kl^4 \quad (21)$$

where k is a constant.

When the mass density of the tumor is relatively homogeneous, we assume proportional relation between the mass and volume:

$$m \propto v \quad (22)$$

When l_0 is the average asymptotic length of the circulatory network of the organ, and M is the asymptotic mass, from (21) and (22) with other K constant:

$$M = Kl_0^4 \quad (23)$$

Consequently, from (23) and (21), we obtain:

$$r = \left(\frac{m}{M} \right)^{1/4} = \left(\frac{Kl^4}{Kl_0^4} \right)^{1/4} = \frac{l}{l_0} \quad (24)$$

The fourths-root of the relative mass growth to the asymptotic value (the relative basal metabolic rate) corresponds to the relative ratio of the length of the circulatory network. The geometrical parameter of the vascularity offers a more

evident intrinsic factor than the mass. The length looks essential in the allometric relations.

From (20) and (24) the geometric growth rate is obtained, where a universal law can describe the average relative length of the circulatory network:

$$r(\tau) = 1 - e^{-\tau}, \quad \tau = \frac{at}{4M^{1/4}} - \ln(1 - r_0) \quad (25)$$

where $r_0 = \left(\frac{m_0}{M}\right)^{1/4}$. The ratio of the energy maintaining new cells is

$R(\tau) = (1 - r(\tau)) = e^{-\tau}$. Assuming the average density of the cancerous cell colony in the experiments of Bru *et al.* [47], the scaling law could be determined by the characteristic lengths, which are (at $\alpha = 3/4$ [45]), $m \propto L^4$ in ideal cases, consequently:

$$r(\tau) = \left(\frac{m}{M}\right)^{1-\alpha} = \left(\frac{L^4}{L_0^4}\right)^{1/4} = \frac{L}{L_0} = 1 - e^{-\tau} \quad (26)$$

where L_0 is the asymptotic size of the cancer-cell cluster. It is naturally assumed that $L_0 \gg L$, then from equation (17) the Taylor expansion of τ could be truncated at its second term, so (26) will be the linear dependence as measured:

$$L(t) \cong \frac{a}{4K}t - L_0 \ln\left(1 - \frac{L(\tau=0)}{L_0}\right) \quad (27)$$

However, if the energy supply is not ideal (which is the case in almost all the developed tumors *in-vivo*), the results do not support the ideal scaling by $\alpha = 3/4$ [38]. It is shown in a generalized model that the fractal surface and the covered volume are scaled rigorously [48].

In cases of sub-optimal alimentation (there is an energy-deficiency for optimal growth), the scaling-exponent changes, and it depends on the fractal dimension of the vascular network (D_v) [48]. The shortage of energy for adequate alimentation is a usual condition for the rapidly proliferating structures. Two strategies can be followed to distribute the available (sub-optimal) energy resources: maximizing the metabolism on the surface of the cells. The elongation of the vascular network (angiogenesis) is the optimal strategy in this growing phase of the tumor ($\alpha_1 = \frac{3}{3+D_{v1}}$) [49]. The optimizing strategy could change in the

advanced stages when the blood volume is limited despite the elongated vascular possibilities. In the advanced cases, the energy-distribution request a $\alpha_2 = \frac{4-D_{v2}}{4}$ exponent ($\alpha_2 < \alpha_1, D_v > 1$) [49]. The growth of the mass would be in these cases (as described by (16)):

$$\frac{dm_{\max}^{(1)}}{dt} = \frac{aD_{v1}}{(3+D_{v1})M^{\frac{D_{v1}}{3+D_{v1}}}} \left(1 - \left(\frac{m}{M}\right)^{\frac{D_{v1}}{3+D_{v1}}}\right) \quad (28)$$

and

$$\frac{dm_{\max}^{(2)}}{dt} = \frac{aD_{v2}}{4M^{\frac{4-D_{v2}}{4}}} \left(1 - \left(\frac{m}{M} \right)^{\frac{4-D_{v2}}{4}} \right) \tag{29}$$

The generalized form of relation (25) could be used in $\alpha_2 < \alpha_1, (D_{v1}, D_{v2} > 1)$ exponents, when the allometry exponent is α . The phase 1 and phase 2 stages of tumors had been studied by various publications [49] [50] [51]. We choose two characteristic values to demonstrate the differences, $D_{v1} = 1.28$ and $D_{v2} = 1.52$.

The time development well shows the different saturation time of the processes with various exponents (Figure 1).

The mass and the characteristic length are strictly connected:

$$m_{\max}^{(1)} = Kl^{\frac{3+D_v}{D_v}} \quad \text{and} \quad m_{\max}^{(2)} = Kl^{\frac{4-D_v}{4}} \tag{30}$$

In general:

$$M = Kl_0^{1-\alpha} \tag{31}$$

and therefore:

$$r = \left(\frac{m_{\max}}{M} \right)^{1-\alpha} = \frac{l}{l_0} \tag{32}$$

For optimal distribution, we get the exact same result:

$$r = \left(\frac{m_{opt}}{M} \right)^{1-\alpha} = \frac{l}{l_0} \tag{33}$$

The limited nutrition, the energetic control of the tumor could be considered as a part of the controlled therapy [52]. If the cell culture were to be placed on the tumour region, and the cell culture had the same or higher demands as the

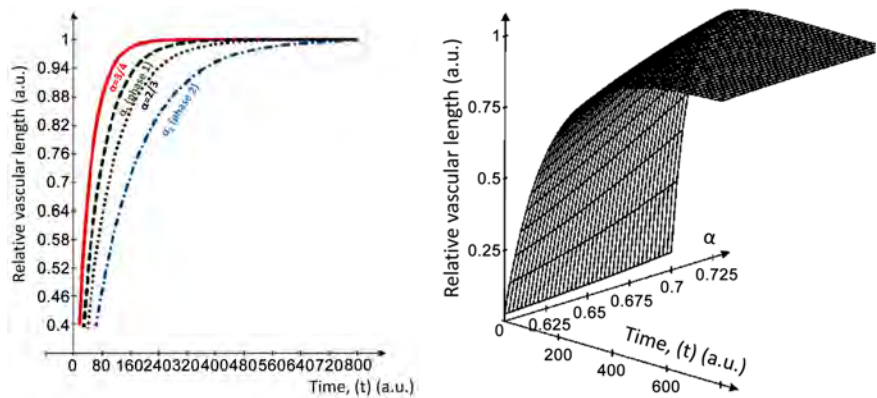


Figure 1. Development of the relative length in time of vascular structure in a tumor at various allometric exponents: the normal, tumor-free tissue $\alpha = 3/4$ (solid line) and in the Euclidean geometrical construction $\alpha = 2/3$ (dotted line). The saturation time to reach the final length increases by the decreasing of the vascular fractal-dimension, ($\alpha_1 = 0.701$, dashed line; and $\alpha_2 = 0.62$, dash-dotted line). The chosen sample parameters: $m_0 = 1$ a.u. and $M = 1000$ a.u. .

tumour tissue, then it could successfully compete against the cancer cells supplied from the same sources of energy. These in-silico results have not yet been verified experimentally, they are expected in the future.

5. Conclusions

The mass change to the more fundamental length of the vascular network in allometric scaling is generally proven in optimal metabolic conditions. We had shown the application in two basic kinds of non-optimal alimentation processes, too.

We proved that allometric scaling could eliminate the mass and an entirely intrinsic parameter, the average relative length of the circulatory network. The allometric model by the length directly connects the metabolic energy intake of the tumor with the length of the vascular system, as a supplier of energy. The derivation of the equations is rather general because the obtained fractal dimensions are model-independent. We regard the vascular length as more fundamental than the mass because the tumor volume is usually indefinitely smeared out, having a gradient formed by the mix of the precancerous and host cells. Hence, the fractal determination of the vascular network gives a more precise solution for allometric relations.

Acknowledgements

This work was supported by the Hungarian National Research Development and Innovation Office PIACI KFI grant: 2019-1.1.1-PIACI-KFI-2019-00011.

Conflicts of Interest

The author declares no conflicts of interest regarding the publication of this paper.

References

- [1] Sornette, D. (2000) *Chaos, Fractals, Self-Organization and Disorder: Concepts and Tools*. Springer Verlag, Berlin.
- [2] Walleczek, J. (2000) *Self-Organized Biological Dynamics & Nonlinear Control*. Cambridge University Press, Cambridge. <https://doi.org/10.1017/CBO9780511535338>
- [3] Kauffman, S.A. (1993) *The Origins of Order: Self-Organization and Selection in Evolution*. Oxford University Press, New York. https://doi.org/10.1007/978-94-015-8054-0_8
- [4] West, B.J. (1990) *Fractal Physiology and Chaos in Medicine*. World Scientific, Singapore.
- [5] Bassingthwaighte, J.B., Leibovitch, L.S. and West, B.J. (1994) *Fractal Physiology*. Oxford University Press, New York. <https://doi.org/10.1007/978-1-4614-7572-9>
- [6] Brown, J.H. and West, G.B. (2000) *Scaling in Biology*. Oxford University Press, Oxford.
- [7] Brown, J.H., West, G.B. and Enquist, B.J. (2005) *Yes, West, Brown and Enquist's*

- Model of Allometric Scaling Is Both Mathematically Correct and Biologically Relevant. *Functional Ecology*, **19**, 735-738. <https://doi.org/10.1111/j.1365-2435.2005.01022.x>
- [8] West, B.J. (2006) Where Medicine Went Wrong: Rediscovering the Path to Complexity. World Scientific, London. <https://doi.org/10.1142/6175>
- [9] West, D. and West, B.J. (2012) On Allometry Relations. *International Journal of Modern Physics B*, **26**, 116-171. <https://doi.org/10.1142/S0217979212300101>
- [10] Deering, W. and West, B.J. (1992) Fractal Physiology. *IEEE Engineering in Medicine and Biology*, **11**, 40-46. <https://doi.org/10.1109/51.139035>
- [11] Kleiber, M. (1961) *The Fire of Life: An Introduction to Animal Energetics*. Wiley, Hoboken.
- [12] Tannock, I.F. (1968) The Relation Between Cell Proliferation and the Vascular System in a Transplanted Mouse Mammary Tumour. *British Journal of Cancer*, **22**, 258-273. <https://doi.org/10.1038/bjc.1968.34>
- [13] Milotti, E., Vyshemirsky, V., Sega, M. and Chignola, R. (2012) Interplay between Distribution of Live Cells and Growth Dynamics of Solid Tumours. *Scientific Reports*, **2**, Article No. 990. <https://doi.org/10.1038/srep00990>
- [14] Guiot, C., Delsanto, P.P.P., Carpinteri, A., *et al.* (2006) The Dynamic Evolution of the Power Exponent in a Universal Growth Model of Tumors. *Journal of Theoretical Biology*, **240**, 459-463. <https://doi.org/10.1016/j.jtbi.2005.10.006>
- [15] West, G.B., Brown, J.H. and Enquist, B.J. (1990) The Four Dimension of Life: Fractal Geometry and Allometric Scaling of Organisms. *Science*, **284**, 1677-1679. <https://doi.org/10.1126/science.284.5420.1677>
- [16] Labra, F.A., Marquet, P.A. and Bozinovic, F. (2007) Scaling Metabolic Rate Fluctuations. *Proceedings of the National Academy of Sciences of the United States of America*, **104**, 10900-10903. <https://doi.org/10.1073/pnas.0704108104>
- [17] West, G.B. and Brown, J.H. (2000) *Scaling in Biology*. Oxford University Press, Oxford.
- [18] Calder, W.A. III (1996) *Size, Function and Life History*. Dover Publications Inc., Mineola.
- [19] Schlesinger, M.S. (1987) Fractal Time and 1/f Noise in Complex Systems. *Annals of the New York Academy of Sciences*, **504**, 214-228. <https://doi.org/10.1111/j.1749-6632.1987.tb48734.x>
- [20] Bak, P., Tang, C. and Wiesenfeld, K. (1988) Self-Organized Criticality. *Physical Review A*, **38**, 364-373. <https://doi.org/10.1103/PhysRevA.38.364>
- [21] Musha, T. and Sawada, Y. (1994) *Physics of the Living State*. IOS Press, Amsterdam.
- [22] Berryman, M.J., Spencer, S.L., Allison, A. and Abbott, D. (2004) Fluctuations and Noise in Cancer Development. *Proceedings of SPIE—The International Society for Optical Engineering*, **5471**. <https://doi.org/10.1117/12.546641>
- [23] Qui, B., Zhou, T. and Zhang, J. (2020) Stochastic Fluctuations in Apoptotic Threshold of Tumor Cells Can Enhance Apoptosis and Combat Fractional Killing. *Royal Society Open Science*, **7**, Article ID: 190462. <https://doi.org/10.1098/rsos.190462>
- [24] Fiasconaro, A., Ochab-Marcinek, A., Spagnolo, B. and Gudowska-Nowak, E. (2008) Monitoring Noise-Resonant Effects in Cancer Growth Influenced by External Fluctuations and Periodic Treatment. *Physics of Condensed Matter*, **65**, 435-442. <https://doi.org/10.1140/epjb/e2008-00246-2>
- [25] Chan, A. and Tuszynski, J.A. (2016) Automatic Prediction of Tumour Malignancy in Breast Cancer with Fractal Dimension. *Royal Society Open Science*, **3**, Article ID:

160558. <https://doi.org/10.1098/rsos.160558>
- [26] Tambasco, M. and Magliocco, A.M. (2008) Relation between Tumor-Grade and Computed Architectural Complexity in Breast Cancer Specimens. *Human Pathology*, **39**, 740-746. <https://doi.org/10.1016/j.humpath.2007.10.001>
- [27] Pamatmat, M.M. (1983) Measuring Aerobic and Anaerobic Metabolism of Benthic Infauna under Natural Conditions. *Journal of Experimental Zoology*, **228**, 405-413. <https://doi.org/10.1002/jez.1402280303>
- [28] Moses, M.E., Hou, C., Woodruff, W.H., *et al.* (2008) Revisiting a Model of Ontogenetic Growth: Estimating Model Parameters from Theory and Data. *The American Naturalist*, **171**, 632-645. <https://doi.org/10.1086/587073>
- [29] Voet, D., Voet, J.G. and Pratt, C.W. (2006) *Fundamentals of Biochemistry*. 2nd Edition, John Wiley and Sons, Inc., Hoboken.
- [30] West, G.B. and Brown, J.H. (2005) The Origin of Allometric Scaling Laws in Biology from Genomes to Ecosystems: Towards a Quantitative Unifying Theory of Biological Structure and Organization. *Journal of Experimental Biology*, **208**, 1575-1592. <https://doi.org/10.1242/jeb.01589>
- [31] West, G.B., Woodruff, W.H. and Born, J.H. (2002) Allometric Scaling of Metabolic Rate from Molecules and Mitochondria to Cells and Mammals. *Proceedings of the National Academy of Sciences of the United States of America*, **99**, 2473-2478. <https://doi.org/10.1073/pnas.012579799>
- [32] West, G.B., Brown, J.H. and Enquist, B.J. (2004) Growth Models Based on First Principles or Phenomenology? *Functional Ecology*, **18**, 188-196. <https://doi.org/10.1111/j.0269-8463.2004.00857.x>
- [33] Banavar, J.R., Damuth, J., Maritan, A., *et al.* (2002) Modelling Universality and Scaling. *Nature*, **420**, 626. <https://doi.org/10.1038/420626a>
- [34] West, G.B., Enquist, B.J. and Brown, J.H. (2002) Modelling Universality and Scaling—REPLY. *Nature*, **420**, 626-627. <https://doi.org/10.1038/420626b>
- [35] Stevens, C.F. (2009) Darwin and Huxley Revisited: The Origin of Allometry. *Journal of Biology*, **8**, Article No. 14. <https://doi.org/10.1186/jbiol119>
- [36] Delides, A., Panayiotides, I., Alegakis, A., *et al.* (2005) Fractal Dimension as a Prognostic Factor for Laryngeal Carcinoma. *Anticancer Research*, **25**, 2141-2144.
- [37] Guiot, C., Degiorgis, P.G., Delsanto, P.P., *et al.* (2003) Does Tumor Growth Follow a “Universal Law”? *Journal of Theoretical Biology*, **225**, 147-151. [https://doi.org/10.1016/S0022-5193\(03\)00221-2](https://doi.org/10.1016/S0022-5193(03)00221-2)
- [38] Deisboeck, T.S., Guiot, C., Delsanto, P.P., *et al.* (2006) Does Cancer Growth Depend on Surface Extension? *Medical Hypotheses*, **67**, 1338-1341. <https://doi.org/10.1016/j.mehy.2006.05.029>
- [39] Nagy, J.A., Chang, S.-H., Shih, S.-C., Dvorak, A.M. and Dvorak, H.F. (2010) Heterogeneity of the Tumor Vasculature. *Seminars in Thrombosis and Hemostasis*, **36**, 321-331. <https://doi.org/10.1055/s-0030-1253454>
- [40] Herman, A.B., van Savage, M. and West, G.B. (2011) A Quantitative Theory of Solid Tumor Growth, Metabolic Rate and Vascularization. *PLoS ONE*, **6**, e22973. <https://doi.org/10.1371/journal.pone.0022973>
- [41] Haanen, C. and Vermes, I. (1996) Apoptosis: Programmed Cell Death in Fetal Development. *European Journal of Obstetrics & Gynecology and Reproductive Biology*, **64**, 129-133. [https://doi.org/10.1016/0301-2115\(95\)02261-9](https://doi.org/10.1016/0301-2115(95)02261-9)
- [42] Kerr, J.F.R., Wyllie, A.H. and Currie, A.R. (1972) Apoptosis: A Basic Biological Phenomenon with Wide-Ranging Implications in Tissue Kinetics. *British Journal of Cancer*, **26**, 239-257. <https://doi.org/10.1038/bjc.1972.33>

- [43] Lowe, S.W. and Lin, A.W. (2000) Apoptosis in Cancer. *Carcinogenesis*, **21**, 485-495. <https://doi.org/10.1093/carcin/21.3.485>
- [44] Karsch-Bluman, A., Feiglin, A., Arbib, E., Stern, T., Shoval, H., Schwob, O., Berger, M. and Benny, O. (2018) Tissue Necrosis and Its Role in Cancer Progression. *Oncogene*, **38**, 1920-1935. <https://doi.org/10.1038/s41388-018-0555-y>
- [45] West, G.B., Brown, J.H. and Enquist, B.J. (2001) A General Model for Ontogenetic Growth. *Nature*, **413**, 628-631. <https://doi.org/10.1038/35098076>
- [46] von Bertalanffy, L. (1957) Quantitative Laws of Metabolism and Growth. *The Quarterly Review of Biology*, **32**, 217-231. <https://doi.org/10.1086/401873>
- [47] Bru, A., Albertos, S., Subiza, J.L., Asenjo, J.L.G. and Bru, I. (2003) The Universal Dynamics of Tumor Growth. *Biophysical Journal*, **85**, 2948-2961. [https://doi.org/10.1016/S0006-3495\(03\)74715-8](https://doi.org/10.1016/S0006-3495(03)74715-8)
- [48] Szasz, A. (2021) Vascular Fractality and Alimentation of Cancer. *International Journal of Clinical Medicine*, **12**, 279-296.
- [49] di Leva, A., Bruner, E., Widhalm, G., Michev, G., Tschabitscher, M. and Grizzi, F. (2012) Computer-Assisted and Fractal-Based Morphometric Assessment of Microvascularity in Histological Specimens of Gliomas. *Scientific Reports*, **2**, Article No. 429. <https://doi.org/10.1038/srep00429>
- [50] Grizzi, F., Russo, C., Colombo, P., Franceschini, B., Frezza, E.E., *et al.* (2005) Quantitative Evaluation and Modeling of Two-Dimensional Neovascular Network Complexity: The Surface Fractal Dimension. *BMC Cancer*, **5**, 14. <https://doi.org/10.1186/1471-2407-5-14>
- [51] Ceelen, W., Boterberg, T., Smeets, P., Van Damme, N., *et al.* (2007) Recombinant Human Erythropoietin α Modulates the Effects of Radiotherapy on Colorectal Cancer Microvessels. *British Journal of Cancer*, **96**, 692-700. <https://doi.org/10.1038/sj.bjc.6603568>
- [52] Deisboeck, T.S. and Wang, Z. (2008) A New Concept for Cancer Therapy: Out-Competing the Aggressor. *Cancer Cell International*, **8**, 19. <https://doi.org/10.1186/1475-2867-8-19>

The Possible Involvement of Apoptotic Decay of Terminal Deoxynucleotidyl Transferase-Positive Lymphocytes in the Reutilization of the Extracellular DNA Fragments by Surrounding Living Cells

Aleksei N. Shoutko

Department of Fundamental Research, Russian Scientific Center of Radiology and Surgical Technologies, Ministry of Health Care, RF, Saint-Petersburg, Russia

Email: shoutko@inbox.ru

How to cite this paper: Shoutko, A.N. (2021) The Possible Involvement of Apoptotic Decay of Terminal Deoxynucleotidyl Transferase-Positive Lymphocytes in the Reutilization of the Extracellular DNA Fragments by Surrounding Living Cells. *Open Journal of Biophysics*, 11, 371-382. <https://doi.org/10.4236/ojbiphy.2021.114014>

Received: June 30, 2021

Accepted: August 15, 2021

Published: August 18, 2021

Copyright © 2021 by author(s) and Scientific Research Publishing Inc. This work is licensed under the Creative Commons Attribution International License (CC BY 4.0). <http://creativecommons.org/licenses/by/4.0/>



Open Access

Abstract

The migrating TdT⁺ thymocytes can die in other tissues, promoting the surrounding cells' renewing likes holocrine secretion does. To clarify the role of TdT-enzyme for this function of progenitor lymphocytes, their extracellular media with its components included by living cells analyzed *in vitro* before and after *in vivo* irradiation of donor rats. The nucleoid with DNase-sensitive (free) DNA and TdT activity discovered in extracellular media conditioned preliminary by spontaneous apoptotic death of a minor part of the thymocyte's suspension *in vitro*. The penetration of labeled products of non-template synthesis with free DNA' primers from media into cells by pinocytosis confirmed by exogenous polymeric DNA marked artificially. The DNA penetration into cells follows an increase of the cell's viability and acceleration of spontaneous intracellular DNA-synthesis controlled with labeled thymidine uptake. Both phenomena are typical for either the lowest initial concentration of intact cells or their preliminary irradiation *in vivo*. The data point to possible involvement of apoptotic decay of TdT⁺ cells in the reutilization of the extracellular DNA fragments for reparation/regeneration of surrounding living cells.

Keywords

Thymocytes, Apoptosis, Terminal Deoxynucleotidyl Transferase, Extracellular Activity, DNA Synthesis, Precursors, Reutilization

1. Introduction

The fundamental property of circulating HSCs is their beneficial effect on cellular renewal and regeneration of tissues of various histotypes. The components of the lymphoid line of hematopoiesis, such as prolymphocytes of bone marrow and cortical thymocytes, may participate in this morphogenic effect of HSC, too. Only they have a specific marker Terminal deoxynucleotidyl Transferase (TdT). About 15% of the circulating CD34⁺ and CD133⁺ hematopoietic stem cells are TdT positive lymphoid progenitors [1]. Thus, they can participate in all processes of the morphogenesis provided by HSCs in peripheral organs and tissues. The enzyme does not require a template for activity. It catalyzes the incorporation of deoxynucleotides into the 3'-OH termini of single- or double-stranded DNA, using as a primer even short oligodeoxynucleotide of at least three bases. It is generally accepted only that the enzyme acts intracellularly, providing a variety of antigen receptors at the V(D)J junction of gene segment (N-region) by the random import of one of the four Deoxyribonucleotides Monophosphates (dNMP) in it. Therefore, enzyme TdT should belong to the group of intracellular potassium-dependent polymerases as all template-dependent DNA polymerases, losing activity tenfold in extracellular media with a physiological concentration of sodium (≈ 0.15 M NaCl) [2]. However, the function of TdT may be more complex because it does not change in the range of NaCl content for plasma and extracellular media 0.14 M and even increases unexpectedly up to 50% in the media with 0.22 M of Na⁺ [2]. Besides this extracellular property, TdT incorporates a dNMP into primer in the presence of divalent metal ions, for example, Zn²⁺, which basal concentrations level in extracellular media (10 nM) is much higher than that in intracellular space (100 pM) [3]. Moreover, only TdT-positive lymphocytes lose their viability after blocking the 3'-OH primers in their DNA, though the blockers do not affect the viability of TdT-negative cells [4]. Eventually/Yet, antigenic stimulation of circulating T-cells can re-activate V(D)J recombination and re-express the gene TdT, re-rejuvenating the mature cells [5]. The ability of TdT to polymerize both deoxy-deoxyribonucleotides, and ribonucleotides does not confirm its ultimate specificity for V(D)J recombination [6]. All these data indicate the possible function of the TdT-enzyme outside the cells is not in consideration until now [7]. On the other hand, the well-recognized existence of free DNA in extracellular media (exDNA) generally discusses in the context of horizontal gene transfer or, as a source of energy and nutrients to other cells after fragmentation by extracellular DNase, avoiding its possible interaction with extracellular polymerases, like TdT [8] [9].

The circulating cells with this unique enzyme do not yet find a place in the traditional pathophysiological schemes describing the health of mammals. Indeed, this fact seems to be an omission, taking into account the appearance of TdT too far from the bone marrow and thymus, where new vessels arise around artificial scaffolds [10]. In this article, we present data *in vitro* to support the expected trophic function of extracellular TdT.

2. Methods

2.1. Objects

The source of thymocytes were glands of non-in-bread albino male rats (120 - 130 g) taken from animals before, 0.5 and 6 hours after total body X-irradiation in dose 8 Gy at a dose rate of 0.91 Gy/min, a 200 kV, a 15 ma, filters of 0.5 mm Cu and 1.0 mm Al. Thymocytes were isolated in iso-osmotic buffered Hanks Balanced Saline Solution (HBSS) and incubated at 37°C at different cells densities (from 2.5 to 23×10^7 cells/ml) and rotating two times per minute at angle 450 during 15 - 115 minutes. Cell viability controls by trypan blue exclusion at dye's concentration of 0.1%. For conditioning of extra Cellular Media (CM), 23×10^7 cells/ml incubated 60 minutes. After centrifugation ($800 \times g$, 5 min), supernatant adjusts to a NaCl concentration of 0.25 M for an avoiding of template-dependent intracellular transcriptional activities (3 - 4 S DNA directed-DNA polymerase, 6 - 7 polyribosyl adenylic acid-dependent DNA polymerase), and uses after second centrifugation ($1.2 \times 10^5 g$, 60 min) as the source of both natural the extracellular enzyme and the primers (further, conditioned media-CM).

2.2. Analyses of CM with Diethyl-Aminoethyl (DEAE)-Cellulose Paper Chromatography

DEAE-cellulose paper chromatography permits to divide CM onto six fractions which correspond to average molecular weight 6×10^2 (1), 2×10^3 (2), 5×10^4 (3), 1×10^5 (4), 1×10^6 (5), and 5×10^6 (6) Dalton of pure DNA [11]. The presence of free extracellular DNA in the fractions CM was evaluated by photometry in a quartz chamber with optical length 4cm or 10 cm, before and after treatment of the CM with DNase I (Merck; 25 µg/mL, 10 minutes). The DNase-sensitive extra cellular substance with optical density (OD) at 260 nm and extinction coefficients 260/230 and 260/280 ≈ 2 accepted as free endogenous DNA expected to be the primer for the TdT enzyme. The polymeric substances with abnormal extinction coefficients 260/230 and 260/280 classify as a nucleoid. The concentration of free endogenous DNA evaluates as $1 \mu g = 0.02 OD/cm$ of the optical length.

Detection of spontaneous extracellular TdT-activity as result of template-independent monomer's polymerization with endogenous primers performers after the addition into CM of 5×10^{-7} M single substrate (deoxyguanosine triphosphate labeled by tritium [$8\text{-}^3\text{H}$] dGTP, 1.3 Ci/mmol; Perkin Elmer) for 15 - 60 minutes at 37°C. After DEAE chromatography, the radioactivity of CM fractions collects on MF-Millipore Membrane Filter, 0.22/0.45 µm (Merck), washes, dries, and such samples measured in 10 ml scintillation fluid (Ultima Gold, Perkin Elmer, USA) (Hionic Fluor, Packard) by spectrometer Hidex 300SL, Finland) with effectiveness around 17%. Then, a nucleoid's radioactivity infraction normalizes to free DNA found in it by parallel DNase I-analyses.

2.3. Preparation of Exogenous Labeled DNA and Its Uptake by Cells

The exogenous chicken DNA (Reanal, Hungary) were labeled with tritium (^3H -

DNA) by the method of isotopic exchange between hydrogen at C-8 of purine bases of the polymer and hydrogen of heavy-tritium (T)-water (THO) [12] in our modification [13] to simulate a possible biological activity of DNA-like by-products of TdT in CM. Tritium-labeled DNA had a specific radioactivity of about 410 dpm/ μg (*i.e.*, about 60.4 $\mu\text{Ci}/\text{mmol}$ of nucleotides).

Fragmentation of exogenous DNA, if needs, before use was performed in HBSS (Gibco) by ultrasonic set URSK-7H (NE Bauman's Moscow Higher Technical School, Russia) at resonance frequency 26.5 kHz adjusting the exposure time under the control of DEAE-chromatography.

During incubation of cells ($2.7 \times 10^7/\text{mL}$) with prepared ^3H -DNA (2.5 $\mu\text{g}/\text{mL}$) in Hanks solution for 120 minutes at 37°C and constant mixing, aliquot samples of cells, if they were, washes three times with Hanks solution, leases in sodium dodecyl sulfate buffer [14]. DNA isolates by well-recognized method Schmidt and Thangauer [15], and its radioactivity counts with beta-spectrometer Liquimat 220, Picker-Nuclear, USA, as described [13].

2.4. Influence of Extra Cellular DNA on Spontaneous (Not Stimulated) DNA Synthesis in Cells

Spontaneous (non-stimulated) DNA synthesis in intact and irradiated *in vivo* cells 6 hours after exposure (2.7×10^7 cells/mL of Hanks solution) controls by the joint incubation with labeled methyl- ^3H thymidine (^3H -TdR, 26 Ci/mmol, 0.8 $\mu\text{g}/\text{mL}$; MP Biomedicals, Fisher Scientific) during 115 min at 37°C . The cellular DNA in aliquots was isolated, and its radioactivity was measured, as described above. In parallel, the experiment repeats with exogenous unlabelled DNA (2.5 $\mu\text{g}/\text{mL}$) added by the 55th minute of incubation.

2.5. Statistical Analyses

Single parameters were evaluated statistically with the calculation of an average, Standard Deviation (SD) and Standard Error (SE). The average values M were compared using t -criterion and probability p . We described the trends of the aggregate parameters before and after sonication by mathematical functions generated automatically using non-linear approximations in the Excel program.

The coefficient determination R^2 used as a statistical measure of the goodness of fit of the regression line to the data. Satisfactory R^2 values were confirmed using Equation (1) for t -parameter:

$$t = \sqrt{R^2 \times (n - 2) / (1 - R^2)} \quad (1)$$

3. Results

Figure 1 shows the extracellular nucleoid in conditioned media (CM) of normal and injured thymocytes CM of normal cells obtained from intact animals after shame-irradiation (a) as well as CM since 0.5 (b) and 6 hours after irradiation (c) have the different fractions of nucleoid with absorption at 260 nm wavelength. DNase-sensitive parts of nucleoid are free DNA. Application only in lower the

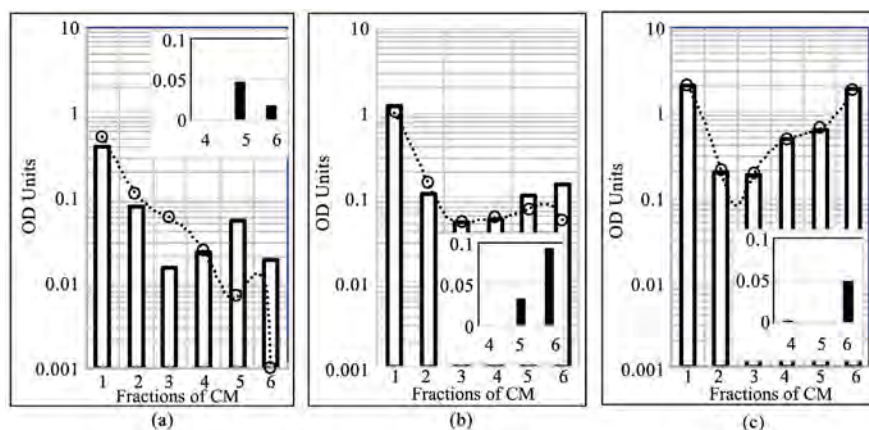


Figure 1. The extracellular nucleoid in thymocytes' CM from animals sacrificed before (a), since 0.5 (b), and 6 hours (c) after single total body X-irradiation of rats at dose 8 Gy. Abscissa: ascending numbers of DNA-like fractions with average molecular weight (Mw) 5×10^2 , 2×10^3 , 5×10^4 , 1×10^5 , 1×10^6 , and 5×10^6 Daltons, according to a CM' fractionation on DEAE-paper. Ordinate: Units of Optical Density (OD Units) at 260 nm received at 4 cm of optical length. Columns-base data before DNase treatment. Circles with dotted lines-the data after DNase treatment. Columns' data satisfy only one or none of two additional ratios ($OD_{260}/OD_{230} \geq 2$ and $OD_{260}/OD_{230} \geq 2$) that are typical for free double strand DNA (*i.e.*, these fractions include proteins and monomers of DNA like bases, nucleoside, nucleotides, and their deoxynucleic forms). The pure DNase-sensitive DNA in fractions shown in the boxes like black columns.

average quantities of such DNA were 0.825, 1.55, and 0.665 $\mu\text{g}/\text{ml}$ for normal, and injured cells by 0.5 and 6 hours correspondently. They associate mostly with fraction 5 (1×10^6 Da) before irradiation and fractions 6 (5×10^6 Da) after it, presenting potential primers for enzyme before, 0.5, and 6 hours after irradiation ($\approx 8.3 \times 10^{-1}$, 3.1×10^{-1} , and 1.3×10^{-1} pmol DNA/mL).

Figure 2 shows the kinetics of spontaneous polymerization of ^3H -dTTP on endogenous DNA-primers of CM by (a) time of incubation (minutes), by (b) concentration of DNase-sensitive DNA in CM ($\mu\text{g}/\text{mL}$) without cells in CM (b), and in the presence of them (c).

Taking into account the specific activity of ^3H -dTTP (1.3 Ci/mmol) and effectiveness of counting (17%), the polymerization's activity of TdT in CM were 1.18, 0.080, 5.66 pmol/mL without cells, and 0.316, 0.036, 0.328 pmole/ml with them for before and 0.5, 6 hours after radiation exposure. Then, the cells uptake 0.864 and 0.044, 5.33 pmoles were with effectiveness 76%, 53%, and 92% before, 0.5, and 6 hours after irradiation correspondently (dotted line in **Figure 2(c)**).

The effectiveness of the uptake of labeled enzyme's product by cells depends on the numbers of labeled primers-molecules, in pmoles, but opposes to it bulk quantity of DNA-primers, in μg (**Figure 2(c)**). None of the relation of uptake's effectiveness with the unlabeled primers in pmoles, as well as nucleoid's concentration in terms of absorption at 260 nm wavelength were found. These data point mainly to the consumption of the labeled products after their selective separation from nucleoids, *i.e.* in the form of free polymers.

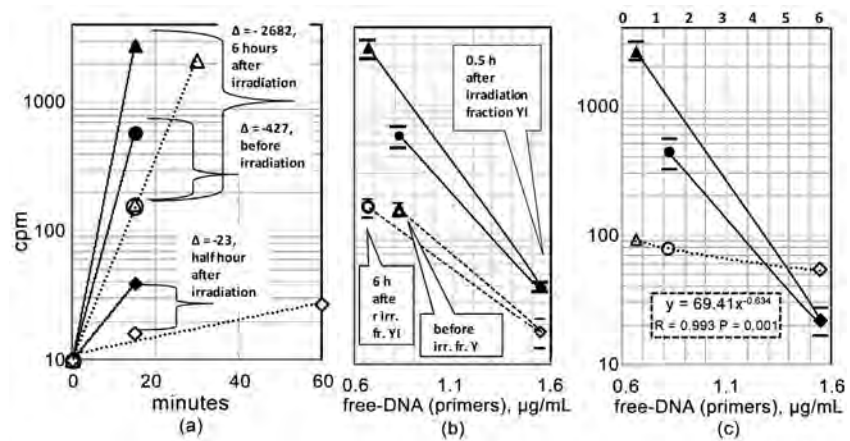


Figure 2. The polymerization of ^3H -dTTP on extracellular DNA-primer in CM of thymocytes from animals sacrificed before (circles), since a 0.5 hour (rhombuses) and 6 hours after (triangles) single total body X-irradiation of rats at dose 8 Gy. Abscissa: (a) time of incubation at 37°C , minutes. (b) and (c) quantity of a DNase-sensitive DNA (free-DNA) in the fractions of nucleoid found by the spectrophotometry and DNase analysis in CM, $\mu\text{g/mL}$. Ordinate: (a), (b) radioactivity of a free DNA-fractions (number 5 and 6) of CM after 15 minutes of incubation, cpm. Dark symbols-CM without cells (WO), white symbols-CM with them (W); (c, black symbols) radioactivity of a free DNA captured by cells as a difference between WO and W results; (c, white symbols, dotted line) effectiveness of a capture as a ratio (WO-W)/W results, %.

Figure 3(a) shows the artificial uptake of pure exogenous DNA (average Mw $\approx 4.5 \times 10^6$ and 1.5×10^5 Da) by intact cells from extracellular media ($6 \mu\text{g/mL}$, *i.e.* $\approx 1.3 \text{ pmol/mL}$ of polymeric molecules and $\approx 40 \text{ pmole/mL}$ of fragmented ones).

According to **Figure 3(a)**, the uptake reaches $0.48 - 0.55 \mu\text{g}$ by maximums, *i.e.* only $\approx 8\% - 9\%$ of the extracellular amount, independently of the difference of Mw. But the *number* of captured molecules of polymeric DNA ($1 \times 10^{-1} \text{ pmol}$) is significantly less than the fragmented one (3.6 pmol). It is remarkable that the longer the time of conditioning the extracellular media is, the less the quantity of captured DNA is registered (**Figure 3(a)**). It is a sign of the wholeness of the uptake, *i.e.*, an intracellular equilibrium between polymeric (acid-insoluble, reutilized) and degraded (acid-soluble) forms.

According to **Figure 3(c)**, the transfer ($\Delta 90$) of exogenous DNA from media into cells 6 hours after their irradiation (8.7% , $1.1 \times 10^{-1} \text{ pmole}$) is comparable with that for intact cells (6.1% , $7.9 \times 10^{-2} \text{ pmol}$) in **Figure 3(b)**. Thus, data 3b and 3c proof the ability of cells to consume large amounts of free DNA from extracellular space.

Does the template-free extracellular polymerization of deoxinucleotides, on the one hand, and consumption of the polymeric forms of DNA by cells, on the other hand, affect the viability of the cells, being the steps of a common mechanism?

Figure 4(a) shows that the low viability of cells at low concentration can be improved by conditioned media up to the level typical for cells suspension concentrated more than a hundredfold.

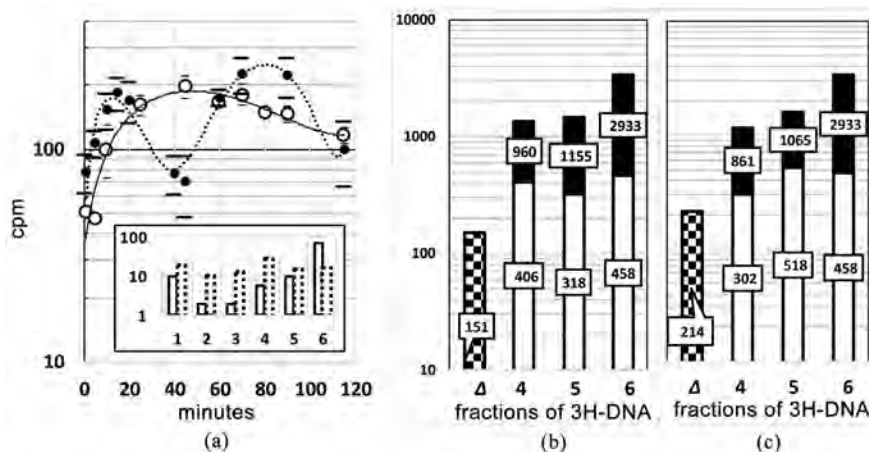


Figure 3. The uptake of exogenous ^3H -DNA ($6 \mu\text{g}/\text{mL}$) by thymocytes ($2.5 \times 10^7/\text{mL}$) from conditioned media (a) and spontaneous fragmentation of ^3H -DNA outside the cells by 90th minute of incubation. Abscissa: (a) time of incubation of exogenous DNA with intact cells, minutes; (b) and (c) DEAE-fractions of ^3H -DNA in conditioned media for intact cells (b) and cells 6 hours after their irradiation *in vivo* (c). White and black columns—fractions 5 and 6 correspondently, other fractions are not shown; B—original ^3H -DNA before incubation ($M_w \approx 4.5 \times 10^6$ Da), WO and W— ^3H -DNA by 90th minute of incubation in media without cells (WO) or with them (W); Δ —total ^3H -DNA captured by cells by 90th minute of the incubation. Ordinate: (a) radioactivity of acid-insoluble fraction of cells' DNA, cpm. In the box: solid line—fractions of original (before incubation) ^3H -DNA ($M_w \approx 4.5 \times 10^6$ Da), dotted line—original ^3H -DNA after preliminary fragmentation ($M.w. \approx 1.5 \times 10^5$ Da), % in the media. (b) and (c) radioactivity of DEAE-fractions of labeled exogenous DNA in CM by 90th minute of incubation, cpm in white boxes. Patterned columns—the part of the total labeled DNA captured by cells: $\Delta_{90} = \text{cpm}_{\text{WO}} - \text{cpm}_{\text{W}}$.

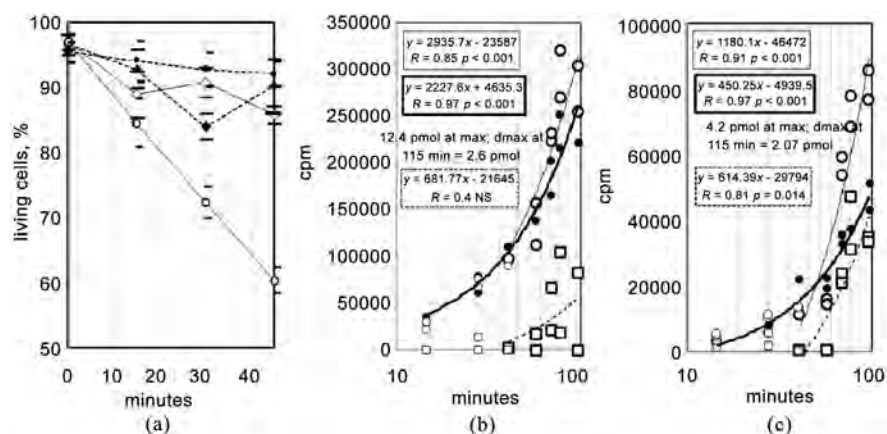


Figure 4. Phenomenon of thymocyte's CM (a) and its simulation with exogenous unlabeled DNA (b) and (c). Abscissa: ((a), (b), (c)) time of incubation, minutes. Ordinate: (a) cells viability, %; circles—unconditioned media (control), rhombuses—preliminary Conditioned Media (CM) by 2×10^7 irradiated cells/ mL ; white symbols— 1×10^5 cells/ mL , black symbols— 2×10^7 cells/ mL ; (b) and (c) radioactivity of ^3H -TdR incorporated into cellular DNA (acid-insoluble fraction). (b)—intact cells, (c)—irradiated *in vivo* cells; thick solid lines—without exogenous DNA, thin solid lines—fragmented DNA, added by 45th minute of incubation; dotted lines—additional ^3H -TdR' uptake in the presence of exogenous DNA. The approximating equations are in the boxes with corresponding line's characters.

A low level of ^3H -TdR incorporation is typical for irradiated cells (**Figure 4(c)**). Only for them, the small amounts of exogenous DNA added to media can increase the ^3H -TdR uptake by cells significantly. The reproducing similar phenomenon with intact cells is impossible, though the same cell concentration (**Figure 4(b)**).

4. Discussion

Intracellular synthesis of dNTP is not autonomy, because missing metabolites or precursors can be imported into cells from neighboring cells or hemolymph. The mechanisms of such a rescue are uncovered [16].

The deficit of the intracellular pool of dNTP in the normal, embryonic and malignant tissues limits strongly cells proliferation via arrest the cycle in S-phase [17] [18]. The six hours after irradiation covers the phenomenon of reversible arrest in cell cycle progression, which is lasting about an hour for every 1 Gy delivered and resulting in a reduced mitotic index [19]. This time corresponds in situ to linear increasing of apoptotic cells number in irradiated gland from 0.8% - 1.8% to 3% - 11% [20], which accompanies by increasing of single-strand breaks (SSB) of cellular DNA [21].

Quick SSB repair by intracellular DNA-polymerase is completed as early as 1 - 0.75 hours after irradiation [22]. The chromatin of rat thymocytes selected 6 hours after total body irradiation, is already cleaved but has still not been eliminated, as one supposed [23]. Therefore, the maximal level of the high polymeric, acid-insoluble nucleoid in the media (**Figure 1**) appears *in vitro* due to the cell's decay at the time of conditioning of CM.

Simultaneously, the maximal concentration of bulk optically active acid-soluble short fractions of nucleoid number 1 increase plainly from control level to 0.5 and 6 hours after irradiation, reflecting the destruction of dead cells during conditioning, which may deliver into CM around 100 - 120 pmol of dNTP per one million lysing cells [24] [25]. Accordingly, at real 6% - 8% apoptotic death of 2.3×10^8 thymocytes/ml, a maximal amount of endogenous dNTP can reach around 2 nmol/mL (2×10^{-6} M) in CM [19]. This amount of substrates is quite compatible with the average natural concentration of precursors of DNA synthesis in plasma and other extracellular fluids (the range of 0.4 - 6 μM) [18].

However, phosphorylating precursors, being negatively charged, are disable penetrate negatively charged cells membrane. One of the possible transporters of needed phosphorylated metabolites inside the cells is pinocytosis, can be thought of as an equal-opportunity importer. It contains surrounding extracellular fluid along with biopolymers and any negatively charged deoxynucleotides into membrane vesicles and imports them easily [26]. The TdT enzyme may be a link in this pathway, leading to restore the intracellular pools of deoxynucleotides and rescue the spontaneous death of young lymphocytes [27]. They migrated into target organs and tissues as lymphoid progenitors with morphogenic (trophic) function [28]. If to consider their apoptosis as physiological suicide (*i.e.* holocrine

type of secretion), then cell-free DNA-primers [29] and TdT enzyme delivered in extracellular media can convert single extracellular deoxynucleotides into oligomers which are captured by neighboring cells, especially if they injured and needed in quick replenishment of exhausted pool of the phosphorylated precursors. Such transfer pinocytosis of blocking precursors is more effective than separated/single ones.

Apart from this general mechanism, the more specific function of TdT might be expected too. Among four deoxynucleosides triphosphate (dNTP), the concentrations of dGTP in dividing cells are 5 - 8 fold lower than in tree others dATP, dCTP, and dTTP [18] [25] [30]. Surprisingly, the preferred order of incorporation by TdT is dGTP > dCTP > dTTP > dATP [31], seeming as a process for compensation of intracellular deficit of dGTP. Tight control of the dNTP pool is essential for cellular homeostasis, especially for deoxyguanosine nucleotides during radiation [32] or chemical damages, for example, the therapeutic toxicant gemcitabine [33]. The deficit dGMP in lymphoid cells follows oxidative stress of different origins when the excess of reactive oxygen species (ROS) modifies normal precourses into mutagen 8-Oxo-7,8-dihydro-2-deoxyguanosine (8-oxo-dG). 8-oxo-dG is removed from the polymer by base excision repair and is excreted into the extracellular environment [34] [35].

Generally recognized the only intracellular function, as noted in the introduction, does not explain several biological features of TdT⁺ cells. Another forgotten but mysterious property of TdT⁺ lymphocytes is their mass and speed emigration from the gland in response to the somatic injury remoted distantly.

In parallel with artificial lymphocytopenia performed by extracorporeal irradiation of circulating blood, 55% of the TdT-positive cortical thymocytes leaves intact gland during 6 hours remotely. The speed of such devastation is highest: fifth-fold faster than the white pulp cells of intact spleen along with yet unchangeable pools of lymph nodes. Thus, by 6 hours after irradiation thymus cells population contains the excess of resistible and slowly mobilizable lymphocytes in medullae though the 45% of rest cortical cells and, probably, the resident progenitors coming from bone marrow, start already the repopulation of the devastated cortex [36].

5. Conclusions

Though the functional outcome of the TdT⁺ cells emigration looks nonsense in the view of intrathymic providing a variety of antigen receptors at the V(D)J junction of gene segment, the feeding/morphogenic function of these circulating cells for renewing the other tissues and organs seems logical. It follows from the property of TdT-positive young emigrating lymphocytes to achieve the other tissues and organs, dies via apoptosis/suicide/holocrine secretion, and take part in the renewing tissues of different histological types [37].

Future studies will undoubtedly shed more insight into the biological role and molecular mechanisms of young lymphocytes transient in different tissues of a body.

Acknowledgements

Aleksei N. Shoutko thanks the Ministry of Health Care of Russian Federation for financial support of this research.

Conflicts of Interest

The author declares no conflicts of interest regarding the publication of this paper.

References

- [1] Azouna, N.B., Berraëis, L., Regaya, Z. and Jenhani, F. (2011) Immunophenotyping of Hematopoietic Progenitor Cells: Comparison between Cord Blood and Adult Mobilized Blood Grafts. *World Journal of Stem Cells*, **3**, 104-112. <https://doi.org/10.4252/wjsc.v3.i11.104>
- [2] Srivastava, B.I.S. (1974) Deoxynucleotide-Polymerizing Enzymes in Normal and Malignant Human Cells. *Cancer Research*, **34**, 1015-1026.
- [3] Haruna, T. and Atsushi, T. (2019) Age-Dependent Modification of Intracellular Zn²⁺ Buffering in the Hippocampus and Its Impact. *Biological and Pharmaceutical Bulletin*, **42**, 1070-1075. <https://doi.org/10.1248/bpb.b18-00631>
- [4] Spigelman, Z., Duff, R., Beardsley, G.P., Broder, S., Cooney, D., Landau, N.R., *et al.* (1988) 2',3'-Dideoxyadenosine Is Selectively Toxic for TdT-Positive Cells. *Blood*, **71**, 1601-1608. <https://doi.org/10.1182/blood.V71.6.1601.1601>
- [5] Zhang, Y., Shi, M., Wen, Q., Luo, W., Yang, Z., Zhou, M., *et al.* (2012) Antigenic Stimulation Induces Recombination Activating Gene 1 and Terminal Deoxynucleotidyl Transferase Expression in a Murine T-Cell Hybridoma. *Cellular Immunology*, **274**, 19-25. <https://doi.org/10.1016/j.cellimm.2012.02.008>
- [6] McElhinny, S.A.N. and Ramsden, D.A. (2003) Polymerase Mu Is a DNA-Directed DNA/RNA Polymerase. *Molecular and Cellular Biology*, **23**, 2309-2315. <https://doi.org/10.1128/MCB.23.7.2309-2315.2003>
- [7] Motea, E.A. and Berdis, A.J. (2010) Terminal Deoxynucleotidyl Transferase: The Story of a Misguided DNA Polymerase. *Biochimica et Biophysica Acta (BBA)—Proteins and Proteomics*, **1804**, 1151-1166. <https://doi.org/10.1016/j.bbapap.2009.06.030>
- [8] Nagler, M., Insam, H., Pietramellara, G. and Ascher-Jenuß, J. (2018) Extracellular DNA in Natural Environments: Features, Relevance and Applications. *Applied Microbiology and Biotechnology*, **102**, 6343-6356. <https://doi.org/10.1007/s00253-018-9120-4>
- [9] Zhivotovsky, B. (2020) Programmed Cell Death: Historical Notes from Russia. *Biochemistry (Moscow)*, **85**, 1127-1133. <https://doi.org/10.1134/S0006297920100016>
- [10] Sheehy, E.J., Vinardell, T., Toner, M.E., Buckley, C.T. and Kelly, D.J. (2014) Altering the Architecture of Tissue Engineered Hypertrophic Cartilaginous Grafts Facilitates Vascularisation and Accelerates Mineralisation. *PLoS ONE*, **9**, e90716. <https://doi.org/10.1371/journal.pone.0090716>
- [11] Davila, C. and Charles, P. (1965) The Chromatography of Nucleic Acid Preparations on Deae-Cellulose Paper: I. Fractionation of Deoxyribonucleic Acid on Paper Strips or Centrifuged Paper Pulp. *Journal of Chromatography A*, **19**, 382-395. [https://doi.org/10.1016/S0021-9673\(01\)99474-9](https://doi.org/10.1016/S0021-9673(01)99474-9)
- [12] Doppler-Bernardi, F. and Felsenfeld, G. (1969) *In Vitro* Incorporation of Tritium into Native DNA. *Biopolymers*, **8**, 733-741. <https://doi.org/10.1002/bip.1969.360080604>
- [13] Shoutko, A.N. and Shatinina, N.N. (1974) Effect of the Degree of Polymerization of

- Exogenous DNA on Its Incorporation into Rat Thymocytes *in Vitro*. *Bulletin of Experimental Biology and Medicine*, **77**, 269-271. <https://doi.org/10.1007/BF00802476>
- [14] Sefton, B.M. (2001) Labeling Cultured Cells with ^{32}P , and Preparing Cell Lysates for Immunoprecipitation. *Current Protocols in Protein Science*, **10**, 13.2.1-13.2.8. <https://doi.org/10.1002/0471140864.ps1302s10>
- [15] Shutko, A.N., Shatinina, N.N. and Rakitianskaia, I.A. (1983) Role of Terminal Deoxyribonucleotidyl Transferase in Stimulating Lymphocyte DNA Synthesis as Affected by PHA. *Tsitologiya*, **25**, 1212-1215. (In Russian)
- [16] Liu, B. and Großhans, J. (2019) The Role of dNTP Metabolites in Control of the Embryonic Cell Cycle. *Cell Cycle*, **18**, 2817-2827. <https://doi.org/10.1080/15384101.2019.1665948>
- [17] Kohnken, R., Kodigepalli, K.M. and Wu, L. (2015) Regulation of Deoxynucleotide Metabolism in Cancer: Novel Mechanisms and Therapeutic Implications. *Molecular Cancer*, **14**, Article No. 176. <https://doi.org/10.1186/s12943-015-0446-6>
- [18] Traut, T.W. (1994) Physiological Concentrations of Purines and Pyrimidines. *Molecular and Cellular Biochemistry*, **140**, 1-22. <https://doi.org/10.1007/BF00928361>
- [19] Malkinson, F.D. (1981) Some Principles of Radiobiology: A Selective Review. *Journal of Investigative Dermatology*, **76**, 32-38. <https://doi.org/10.1111/1523-1747.ep12479220>
- [20] Fujita, K., Kawarada, Y., Terada, K., Sugiyama, T., Ohyama, H. and Yamada, T. (2000) Quantitative Detection of Apoptotic Thymocytes in Low-Dose X-Irradiated Mice by an Anti-Single-Stranded DNA Antibody. *Journal of Radiation Research*, **41**, 139-149. <https://doi.org/10.1269/jrr.41.139>
- [21] Ivannik, B.P., Golubeva, R.V., Proskuryakov, S.Y. and Ryabchenko, N.J. (1975) Repair and Degradation of DNA in the Irradiated Rat Thymocytes. *Radiobiologiya*, **15**, 500-505. (Article in Russian)
- [22] Tempel, K. (1990) Changes in Nucleoid Viscosity Following X-Irradiation of Rat Thymic and Splenic Cells *in Vitro*. *Radiation and Environmental Biophysics*, **29**, 19-30. <https://doi.org/10.1007/BF01211232>
- [23] Pechatnikov, V.A., Afanasyev, V.N., Korol, B.A., Korneev, V.N., Rochev, Yu.A. and Umansky, S.R. (1986) Flow Cytometry Analysis of DNA Degradation in Thymocytes of γ -Irradiated or Hydrocortisone Treated Rats. *General Physiology and Biophysics*, **5**, 273-284.
- [24] Qiu, X., Guittet, O., Mingoies, C., El Banna, N., Huang, M.-E., Lepoivre, M. *et al.* (2019) Quantification of Cellular Deoxyribonucleoside Triphosphates by Rolling Circle Amplification and Förster Resonance Energy Transfer. *Analytical Chemistry*, **91**, 14561-14568. <https://doi.org/10.1021/acs.analchem.9b03624>
- [25] Huang, C.-Y., Yagüe-Capilla, M., González-Pacanoska, D. and Chang, Z.-F. (2020) Quantitation of Deoxynucleoside Triphosphates by Click Reactions. *Scientific Reports*, **10**, Article No. 611. <https://doi.org/10.1038/s41598-020-57463-3>
- [26] Desai, A.S., Hunter, M.R. and Kapustin, A.N. (2019) Using Macropinocytosis for Intracellular Delivery of Therapeutic Nucleic Acids to Tumor Cells. *Philosophical Transactions of the Royal Society B, Biological Sciences*, **314**, Article ID: 20180156. <https://doi.org/10.1098/rstb.2018.0156>
- [27] Mann, C.L., Hughes, F.M. and Cidlowski, J.A. (2000) Delineation of the Signaling Pathways Involved in Glucocorticoid-Induced and Spontaneous Apoptosis of Rat Thymocytes. *Endocrinology*, **141**, 528-538. <https://doi.org/10.1210/endo.141.2.7314>
- [28] Shoutko, A.N., Gerasimova, O.A., Fedorov, V.A. and Zherebtsov, F.K. (2019) Non-Invasive Vibration-Stress of the Cirrhotic Liver of Patients Waiting for Transplantation Induces of Circulating CD133+ Stem Lymphocytes Committed Phenotypi-

- cally toward the Liver. *Open Journal of Biophysics*, **9**, 155-168.
<https://doi.org/10.4236/ojbiphy.2019.93012>
- [29] Hu, Z., Chen, H., Long, Y., Li, P. and Gu, Y. (2021) The Main Sources of Circulating Cell-Free DNA: Apoptosis, Necrosis and Active Secretion. *Critical Reviews in Oncology/Hematology*, **157**, Article ID: 103166.
<https://doi.org/10.1016/j.critrevonc.2020.103166>
- [30] Ferraro, P., Pontarin, G., Crocco, L., Fabris, S., Reichard, P. and Bianchi V. (2005) Mitochondrial Deoxynucleotide Pools in Quiescent Fibroblasts. A Possible Model for Mitochondrial Neurogastrointestinal Encephalomyopathy (MNGIE). *The Journal of Biological Chemistry*, **280**, 24472-24480. <https://doi.org/10.1074/jbc.M502869200>
- [31] Deshpandea, S., Yangb, Y., Chilkotia, A. and Zauschera, S. (2019) Enzymatic Synthesis and Modification of High Molecular Weight DNA Using Terminal Deoxynucleotidyl Transferase. *Methods in Enzymology*, **627**, 163-188.
<https://doi.org/10.1016/bs.mie.2019.07.044>
- [32] Belli, M. and Tabocchini, M.A. (2020) Ionizing Radiation-Induced Epigenetic Modifications and Their Relevance to Radiation Protection. *International Journal of Molecular Sciences*, **21**, Article No. 5993. <https://doi.org/10.3390/ijms21175993>
- [33] Guo, J.-R., Chen, Q.-Q., Lam, C.W.K., Wang, C.-Y., Wong, V., K.W., Chang, Z.-F., et al. (2016) Profiling Ribonucleotide and Deoxyribonucleotide Pools Perturbed by Gemcitabine in Human Non-Small Cell Lung Cancer Cells. *Scientific Reports*, **6**, Article No. 37250. <https://doi.org/10.1038/srep37250>
- [34] Haghdoost, S., Czene, S., Näslund, I., Skog, S. and Harms-Ringdahl, M. (2005) Extracellular 8-oxo-dG as a Sensitive Parameter for Oxidative Stress *in Vivo* and *in Vitro*. *Free Radical Research*, **39**, 153-162. <https://doi.org/10.1080/10715760500043132>
- [35] Sangsuwan, T. and Haghdoost, S. (2008) The Nucleotide Pool, a Target for Low-Dose γ -Ray-Induced Oxidative Stress. *Radiation Research*, **170**, 776-783.
- [36] Cronkite, E.P., Chanana, A.D., Joel, D.D., Rai, K.R. and Schiffer, L.M. (1968) Influence of Extracorporeal Irradiation of the Blood and Lymph on Lymphopoiesis and Immunity. *Proceedings of a Symposium on the Effects of Radiation on Cellular Proliferation and Differentiation*, Monaco, 1-5 April 1968, 307-326.
- [37] Shoutko, A.N. (2019) Immunity or Morphogenesis in Cancer Development and Treatment. *Integrative Cancer Science and Therapeutics*, **6**, 1-8.
<https://doi.org/10.15761/ICST.1000317>

The Mystery on the Physical Conditions for Life

Kai Wai Wong¹, Wan Ki Chow²

¹Department of Physics and Astronomy, University of Kansas, Lawrence, USA

²Department of Building Services Engineering, The Hong Kong Polytechnic University, Hong Kong, China

Email: kww88ng@gmail.com

How to cite this paper: Wong, K.W. and Chow, W.K. (2021) The Mystery on the Physical Conditions for Life. *Open Journal of Biophysics*, 11, 383-396.
<https://doi.org/10.4236/ojbiphy.2021.114015>

Received: August 3, 2021

Accepted: September 3, 2021

Published: September 6, 2021

Copyright © 2021 by author(s) and Scientific Research Publishing Inc. This work is licensed under the Creative Commons Attribution International License (CC BY 4.0).

<http://creativecommons.org/licenses/by/4.0/>



Open Access

Abstract

Based on the Perelmann mappings from the homogenous 5D onto the inhomogeneous Lorentz 4D manifold at liquid water phase temperature range, it is shown that coherent and decoherent molecules, water, carbon, hydrogen and oxygen naturally replace the Quarks in the standard model at Bethe fusion temperature as the SU(3) generators, leading to the formation of nitrogenous bases to house the monopole boson eigenstates that can exist within the RNA and DNA. Through which the growth of organic cells by inducing the Off Diagonal Long-Range Order of “p” type hole states in organic rings and bio-cells and thus “Life”.

Keywords

Perelmann Mappings, RNA, DNA, Coherent and Decoherent Molecules Including Nitrogenous Bases, DNA Segments and Deceases, Intelligence, Senses and Memory

1. Introduction

We had previously proposed that the creation of the universe started with the creation of a homogeneous 5D manifold [1], and obeying the uncertainty principle. Such a manifold [2] then has an enclosing 4D homogenous Maxwell manifold boundary [3]. Because of that, the universe started with a Big Bang, with infinite energy, carried by the Diagonal Long-Range Order (DLRO) monopoles, and photons [4]. Since the monopoles are of DLRO, they must be in the Bose-Einstein ground state [5] [6]. It is this phenomenon that these monopoles are in fact the Higgs Bosons [7]. But because the existence of the simultaneous photons on creation requires the presence of a charge current, and as the monopole magnitude is composed of the direct products of e and $-e$ opposite momenta pairs of massless e -trino, and anti- e -trino, the photons must arise from the natural breaking

of the charge neutrality of the monopoles into equal numbers of massive e and $-e$ Dirac spinors, that obey gauge invariance. It is this necessity so that charge currents can be generated to produce the photons during creation, that we can obtain via the expansion of the Bose distribution for the monopoles in terms of a converging power series of the Boltzmann partition factor, such that we can obtain the massive e and $-e$ particle energies by truncating the lower limit of the Boltzmann factor E/kT , so that we can obtain different temperature depending on mass creations [8], such as the Gell-Mann standard model at Bethe fusion Temperatures, etc. [9], and including at low temperatures where the liquid water phase exists [10]. It is in this temperature range that we found the existence of Life forms on earth. As T decreases so must the cut-off E value. By applying the Perelmann's Ricci-flow entropy mapping, a toroidal Lorentz manifold is created, within time t_o , which then gives the toroidal tube radius $r_o = ct_o$ according to Fermat's sum, but with arbitrary toroidal center hole dimension; implying the Perelmann mapping can be initiated at an arbitrary time after the Big Bang. Hence E_o in the lower cut-off obeying uncertainty is less than h/t_o . Should we accept Geesink's assignment that water represents the basic Cartan identity if the Lorentz space-time toroidal mapped out is completely uniformly occupied only by water molecules, then water's molecular weight of 18 nucleon mass must contain exactly the Cartan identity sum. Furthermore, the Geesink formula for coherent phonon spectra is completely valid.

The Quark model can be obtained by making a conformal projection of the 4th space dimension into the remaining 3 space dimensions [1]. Since projection has no inverse, it is irreversible, so is making a Perelmann-Ricci-flow entropy mapping. Finally by exciting the Bose-Einstein ground state of the monopoles by expanding the Bose distribution in an increasing power series of the Boltzmann partition function and truncating the factor E/kT at a lower limit cut-off for creating masses out of the monopole states is equivalent to the Higgs theory and is also irreversible. Thereby when we consider in the low temperatures, as life forms are created, these monopole states in the bio RNA and DNA systems must also be governed by irreversible geometrical boundaries; from the molecular structures that must contain not only coherent but also decoherent spectra that make up the spectra of the RNAs and DNAs. As life forms are only known to exist in such a low-temperature environment, it would be nice if we can deduce this fact from basic mathematical and physical principles.

2. The Geesink Coherent Molecule

It has always been the most mysterious question to us human as to how and under what necessary conditions can life forms exist on a planet. 75 years ago, Schrodinger the physicist that initiated Quantum Mechanics postulated that "LIFE" is also a quantum phenomenon [11]. Yet this connection remains unanswered. While it is well-known that water plays a necessary and key role. And to this day, we make it our goal to find water on other planets as our condition

for hope of also finding life. More recently, Geesink and Meijer [12] successfully derived a low frequency spectra formula for bio-molecules, starting with water, as represented by a toroidal structure, such that other elements essential to life, such as oxygen, carbon, nitrogen and hydrogen can all be fitted into the same formula, dividing it into coherent and decoherent [13]. Because their formula fit so well to our knowledge of bio-rings, it is very interesting to investigate the Geesink coherent, decoherent spectra formulae which is based on the molecular weight, by standardizing the water molecular weight as 1:

$$E_{n,m,p} = \hbar w_{ref} 2^n 3^m 2^p \quad (1)$$

where w_{ref} is a cell specific frequency, assuming the Debye phonon spectrum dependence $M^{-0.5}$ on the molecular weight M , and p, m are positive and negative integers. $n = 0, 0.5, 2, 4, 5, 7, 8, -1, -3, -4, -6, -7$.

The 0.5 factor comes from hydrogen atomic weight which is $1/2 \times (1/3)^2$ as will become clearer as we discuss the essential molecules for life: water molecular weight as 1 representing the SU(3) generators Cartan identity, together with oxygen and carbon.

$$m = 0, 1, 2, 3, 4, 5, -1, -2, -3, -4, -5.$$

$$p = \langle -4, -4, -3, -2, -1, 0, 1, 2, 3, 4, 5, 6 \rangle 52.$$

The weight of a molecule is overwhelmingly due to the constituents' atomic weight, as the electrons are only of order 1/1000 of the nucleus. Thus, using the proton and neutron weight scale as 1, water has a nucleon weight of $16 + 2 = 18$.

Geesink proposes that water should have a topological shape of a toroidal. According to the SU(3) Cartan identity, it would be in turns of $[2/3]^2 + [2/3]^2 + [-1/3]^2 = 1$. This Cartan Sum Rule then implies a toroidal Lorentz manifold as created out by Perelman Ricci-Flow mapping, with the tube radius represented by 1/3 as shown in **Figure 1** below.

The tube radius 1/3 is in unit of $r_o = ct_o$, where t_o is the Ricci Flow action time.

The toroidal center core radius remains arbitrary, in agreement with Geesink's topological shape [14]. We like to point out that this is in agreement with Perelman-Ricci-flow mapping [15], a necessary topological mapping that will create a 4D Lorentz manifold out of the 5D homogenous manifold.

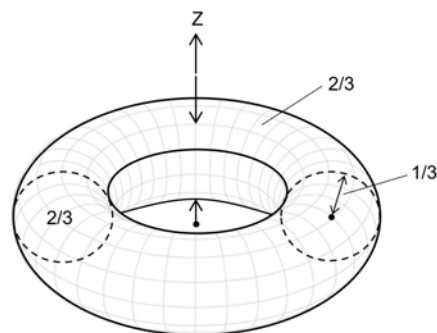


Figure 1. Geesink's toroidal model for water.

Now considering the oxygen O_2 molecule, we have:
 $[32/18] = 1 + 7/9 = 1 + [2/3]^2 + 3[1/3]^2$, which is a toroidal with attachments geometry.

Hydrogen $H_2 = 2/18 = [1/3]^2$ is only line geometry.

The combination water can be expressed as:

$$\left[[16/18] + [1/3]^2 \right] = \left[2(2/3)^2 + (1/3)^2 \right]$$

which is indeed the simple $SU(3)$ toroidal. That means it represents the realized Perelman Ricci-flow mapping, $2D \times 1D$ toroidal space form. Thus the quadratic sum represents such $2D \times 1D$ symmetry, and is not given by the 3D Lorentz gauge. For that to be obeyed, we need the linear sum of the $SU(3)$ generators.

To understand this 3D symmetry, let us investigate the Carbon 12 nucleus [16]. On it, we have 6 protons and 6 neutrons, arranged into three hexagons and 6 equilateral triangles. According to the Gell-Mann standard model, the proton and neutron are the gauge invariant product of three quarks: namely up-up-down and up-down-down. The up Quark has a fractional charge $[2/3]e$, while the down Quark is given by $-[1/3]e$. And $2/3$, $2/3$ and $-1/3$ form the set of $SU(3)$ generators. Thus the gauge invariance restricts the linear sum of these generators to integer. Since carbon 12 nucleus is a spherical object, the gauge implied linear sum rule is applied to 3D space symmetry, and not that of the toroidal geometry [17]. Nonetheless, on the nuclear surface, it is still 2D, and the hexagon and triangles are and must be the mapping result similar to that suggested by Geesink for water. In fact, we can go a step further, and look at the surface of the Bucky Ball. There we found on top of hexagons, we have pentagons, replacing the triangles. It is this very feature in 2D, which we find all the bio-rings are given in terms of hexagons, pentagons and triangles. There are no other geometrical shapes. Hence, the Geesink picture for water indeed should be valid.

Yet choosing water molecular weight as 1 is also equivalent to choosing it to represent the $SU(2)$ Cartan generator 1, which makes the 5D to 4D mapping spherically symmetric. The Oxygen, and Nitrogen atom and molecule however always remain expressed as $SU(3)$ generators only and like carbon are essential to the Lorentz 4D Ricci-flow toroidal mapping. In short for the coherent molecular absorption coherent spectra, water, oxygen, carbon and nitrogen plus hydrogen molecule play the role in determining the $SU(3)$ generators in creation, while odd number of hydrogen atom leads to decoherent absorption, vital to the implement of evolution.

Now consider the molecule $2[CH_3]$, its molecular weight is:

$$30/18 = \left\{ 1 + (2/3)^2 + 2(1/3)^2 \right\} \quad (2)$$

Thus CH_3 is an essential building block of bio-molecules similar to water “plus carbon”.

$2(CH_3)$ as represented in terms of the $SU(3)$ generators is then clearly a coherence molecule. On the other hand, the single CH_3 gives us in units of water $M = [1/2 + 1/3]$. The $1/2$ factor makes it a decoherent molecule. Thus separating

of the two CH₃ in a bio system will cost a breaking of symmetry.

It is this equivalence that allow yeast, a small bio-cell, to convert bio-carbonate powder, *i.e.*, any baking flour, when water is added to create CH₃, and thus gives to a physical rise in the mixture. The reverse is also true, when microwave is applied to baked bread releases water, and becomes moist. All bio-cells including yeast, contains a genome spectrum, thus nitrogenous bases.

Of the most important and interesting bio-rings are therefore the nitrogenous bases that make up the RNAs and DNAs in human.

Let's look at the nitrogenous base Uracil. See **Figure 2** [1].

It contains O₂ + 2H₂ + N₂ + 4C. Thus its molecular weight normalized to water is:

$$\begin{aligned} & \left\{1 + (2/3)^2 + 3(1/3)^2\right\} + 2(1/3)^2 + \left\{1 + (2/3)^2 + (1/3)^2\right\} + 4(2/3) \\ &= \left\{1 + 2(2/3)^2 + 6(1/3)^2 + 4(2/3)\right\} = \left\{2 + 5(1/3)^2 + 6(2/3)^2\right\} \quad (3) \\ &= \left\{3 + 4(1/3)^2 + 4(2/3)^2\right\} = \left\{5 + 2(1/3)^2\right\} \end{aligned}$$

The 2(1/3)² denotes the two different dangling attachments of either O or H to the hexagon vertices. While the 5 denotes the topological degrees of freedom from 3 vertical axis choices + 2 parities of the toroidal structure, represented by the hexagon.

And a clear indication of a toroidal of tube of radius (1/3), similar to water, and is actually resulted from the covariant Carbon in the nitrogenous base. The molecular weight of carbon 2/3 can also be expressed as (2/3)² + 2(1/3)². Meaning it is both symmetric in structure to 3D and 2D × 1D. No other essential elements can do that. Thus due to this, carbon is vital to the formation of bio-rings.

Now let us investigate the corresponding end cap nitrogenous base in the DNA, namely Thymine.

It consists of the same hexagon ring of 4C and 2N, with the change in attachments of 2O, 2H and H₃C. Comparing to Uracil, the only difference is an extra H₂C molecular weight.

$$H_2C = 14/18 = 7/9 = (2/3)^2 + 3(1/3)^2 \quad (4)$$

Thus the weight becomes $\left\{5 + 2(2/3)^2 + (1/3)^2\right\} = 6$ exactly. This exact factor 6 for Uracil corresponds to the 3 vertical axis passing through the 3 adjacent Carbons in the hexagon times the 2 up, down faces differences instead of the 2 additive parities, making it a reflecting end cap on one face, and a transmitting through the reverse side. Such a property is then vital to allow for the monopole boson fields as discussed in our recent paper [14] to go around from one RNA side to loop around to the other RNA and thereby complete a quantum loop.

To further prove the point, let us consider another in between nitrogenous base Cytosine. It differs from Uracil, by missing an H, and replacing a O with NH₂. Thus we get the molecular weight as:

$$\begin{aligned} & \left\{5 + 2(1/3)^2\right\} - (1/3)^2/2 - 2(2/3)^2 + 2(2/3)^2 \\ &= \left\{5 + (3/2)(1/3)^2\right\} = \left\{5 + 3(1/3)^2(1/2)\right\} \quad (5) \end{aligned}$$

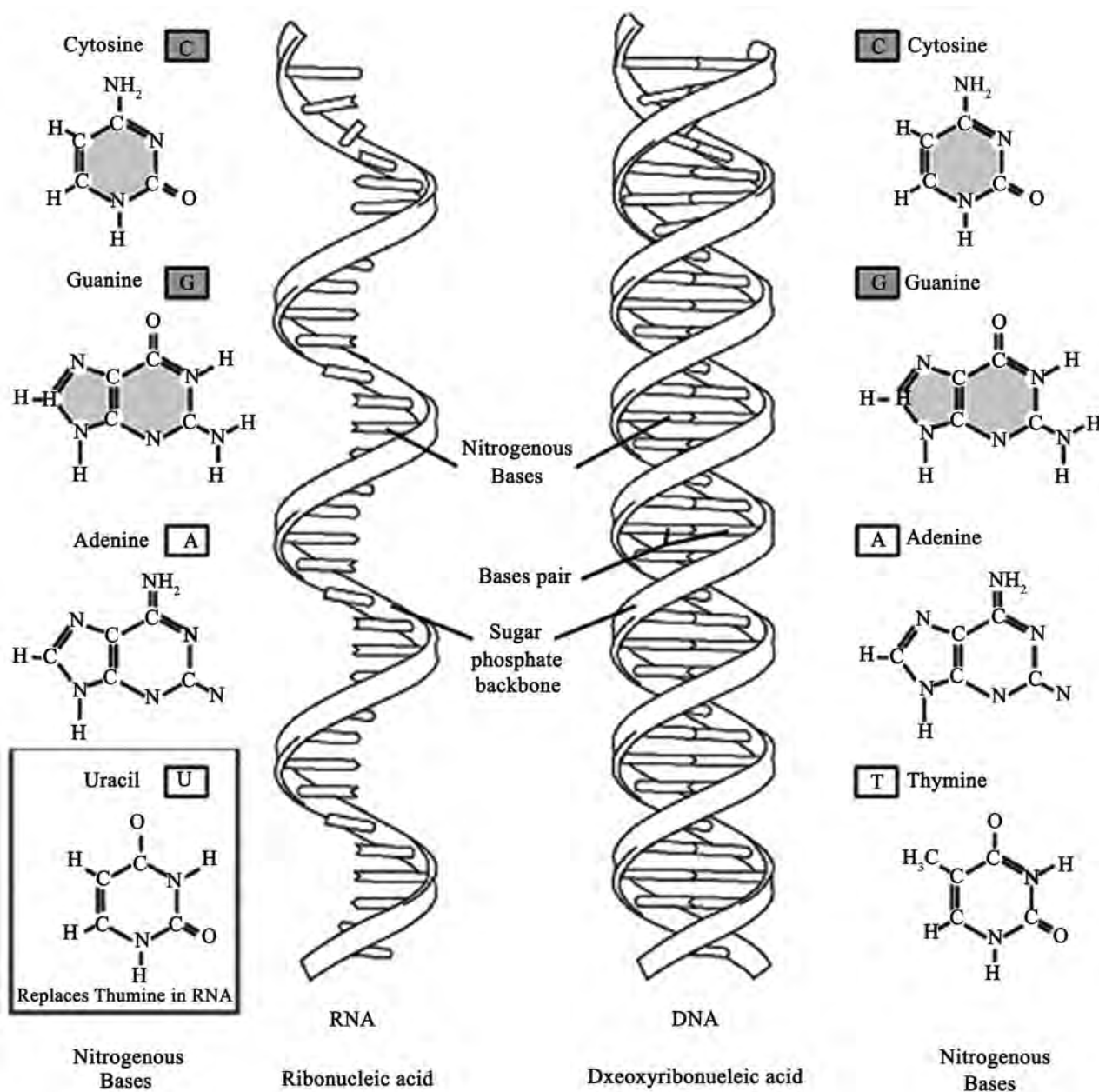


Figure 2. Images of DNA and RNA. Credit: NIH; adapted from national human genome research institute (Wong *et al.* 2014) [1].

The presence of the $(1/2)^3(1/3)^2$ term shows it is a decoherent ring structure, as the factor $1/2$ is not a Cartan generator. While the factor 5 is the degree of freedom 3 Cs and 2 parities.

Lastly let's consider the nitrogenous base Adenine. Compared again to cytosine, we replace O by H , and add CN_2 . We get:

$$\begin{aligned}
 & \{5 + (1/3)(1/2)\} - 2(2/3)^2 + (1/3)^2(1/2) + \left[(2/3) + \{1 + (2/3)^2 + (1/3)^2\} \right] \\
 & = \{6 + (1/2)(2/3)^2 - (2/3)^2 + (2/3) + (1/3)^2\} \tag{6} \\
 & = \{6 + 3(1/3)^2 + (2/3)^2(1/2)\}
 \end{aligned}$$

The factor 6 for the toroidal degrees of freedom of Adenine as compared to the factor 5 for Uracil is the result of the single pentagon attachment, making it having the extra degree of top and bottom, while the factor $3(1/3)^2$ is the result of parity with regard to the 3 perpendicular axis.

Again, Adenine contains a decoherent factor of $(2/3)^2(1/2)$ replacing the $3(1/3)^2(1/2)$ in Uracil.

In fact, the same decoherent factor exists for the remaining nitrogenous base Guanine. The only difference in molecular weight is an extra O and H. Therefore, we have:

$$\begin{aligned} & \left\{ 6 + 3(1/3)^2 + (2/3)^2 (1/2) \right\} + 17/18 \\ &= \left\{ 6 + 3(1/3)^2 + \left[5(2/3)^2 + (1/3)^2 \right] (1/2) \right\} \\ &= \left\{ 6 + 3(1/3)^2 + \left[1 + 3(2/3)^2 \right] (1/2) \right\} \end{aligned}$$

It is vitally important to have the decoherent factor $(1/2)$, for the in-between nitrogenous bases so that the random stacking of all the bases can change and evolve giving rise to evolution and a distinct genome spectrum for each individual life. The decoherent part in Guanine contains a 1, representing the presence of a broken hexagon attachment to the important nitrogenous common carbon ring.

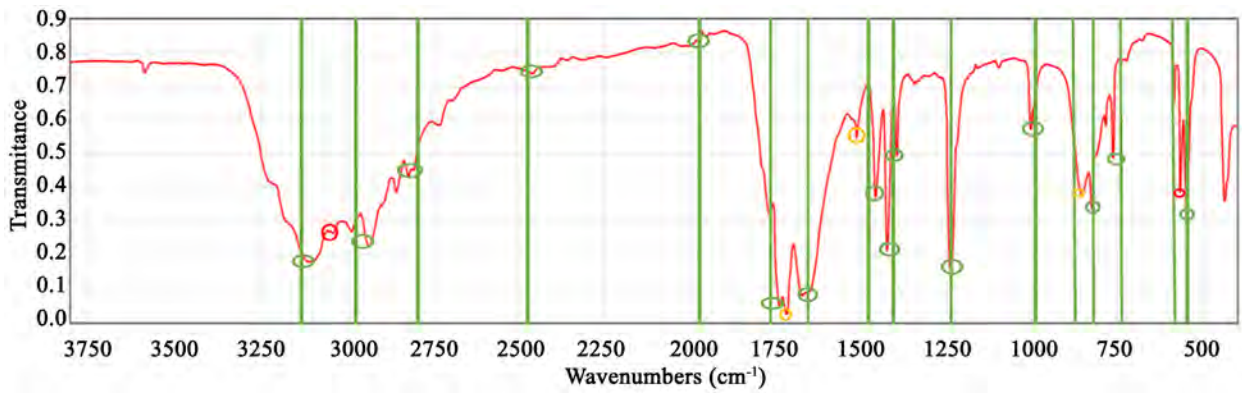
To be able to obtain these nitrogenous bases explicitly from Lie algebra mapping and its relationship to the different atoms will require much more topological mapping knowledge.

Nonetheless we see that Geesink's coherent and decoherent spectra formula indeed appears to be valid and plays a role in the understanding of the quantum aspect of Life as suggested by Schrodinger 75 years ago [18]. The phonon absorption spectra for these 5 nitrogenous bases were published by Geesink [14]. We present it in **Figure 3** [14] simply for completeness.

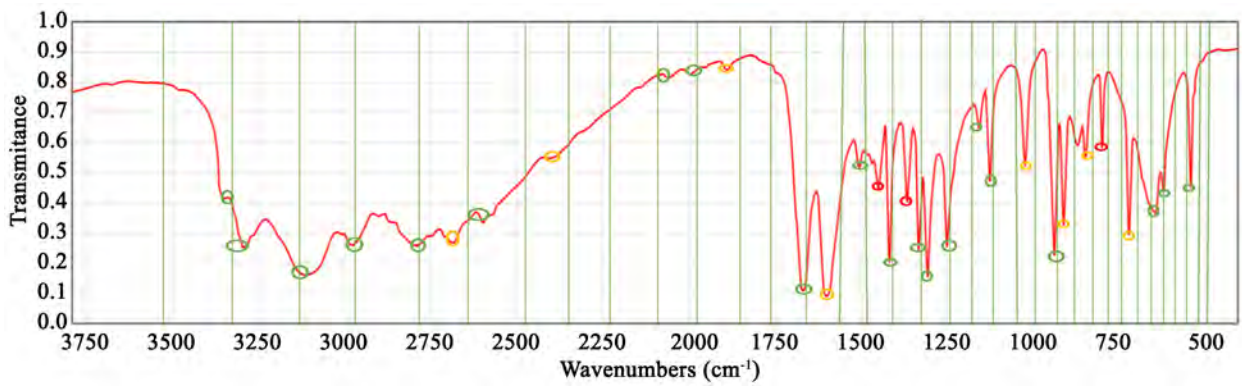
The topological geometry of the nitrogenous bases does not change the quantum monopole loop spectra in the DNA, but it does provide a perturbation boundary condition effect to the DNA twisting itself, thus produces near infinite adjustment modifications possible, which in turn allows for the incoherent effect from the nitrogenous bases to induce the evolution of the life form, a very important physics that is built in for all survival of the fittest (See Chapter 12 of reference 1, for which we will not repeat here).

3. Survival of Life Forms

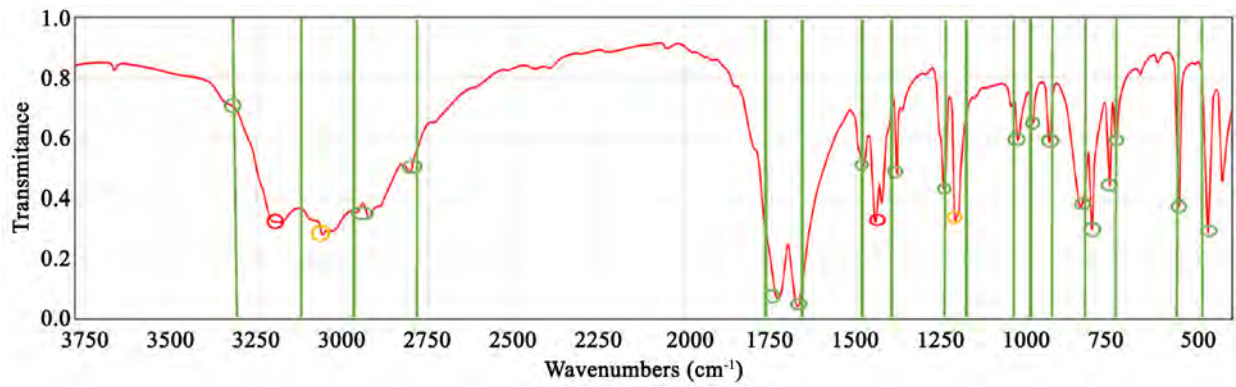
To explain this survival of the fittest, let us consider the general structure of bio-cells. A similar creation of the bio-cells structures similar to the bio-rings geometry would result in point group like structures that also obey $2D \times 1D$ symmetry, which is similar to clay, which is composed of mainly silicon and the High Temperature Ceramic Superconductors [19]. These structures lead to semi-conductor like band structures, with positive band gap between the



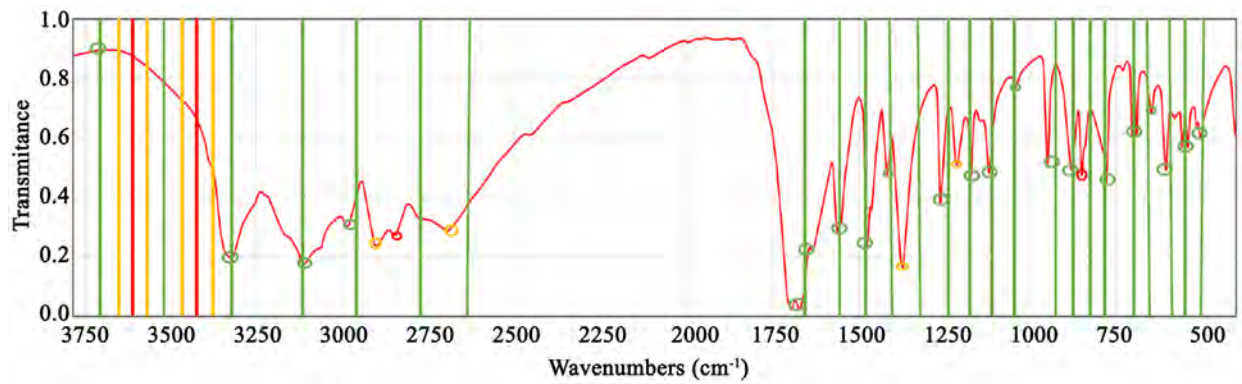
(a)



(b)



(c)



(d)

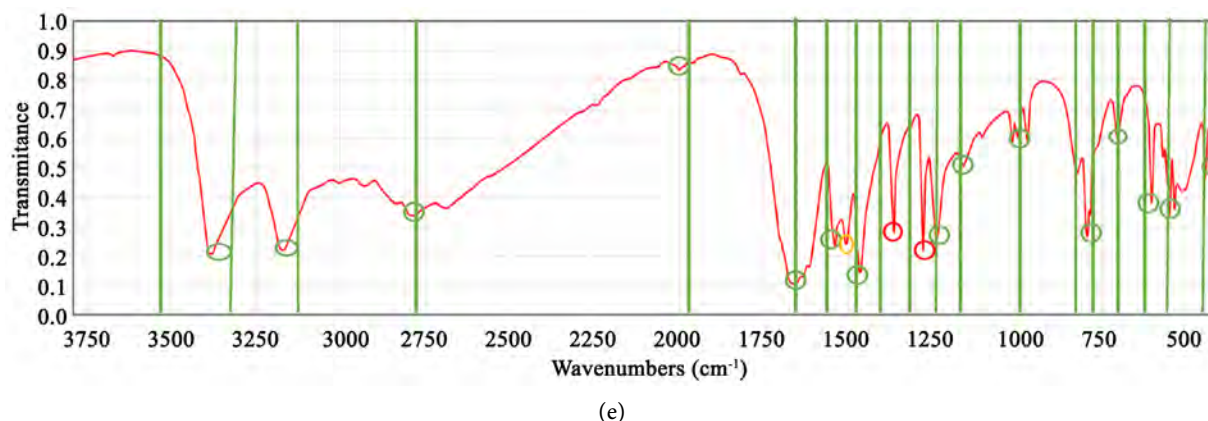


Figure 3. Phonon absorption spectra for the 5 nitrogenous bases (Geesink 2020) [14]. (a) Uracil, NIST. Notice: spectra from this collection were measured on dispersive instruments, often in carefully selected solvents, and hence may differ in detail from measurements on FTIR instruments or in other chemical environments. Remark: Overall pattern is predominantly coherent according to the proposed coherence-scale (green), partly in transition zone (yellow), and some frequencies (red) at decoherent positions; (b) Adenine, NIST. Remark: Overall pattern is predominantly coherent according to the proposed coherence-scale (green), partly in transition zone (yellow), and some frequencies (red) at decoherent positions; (c) Thymine, NIST. Remark: Overall pattern is predominantly coherent according to the proposed coherence-scale (green), partly in transition zone (yellow), and some frequencies (red) at decoherent positions; (d) Guanine, NIST. Remark: Overall pattern is predominantly coherent according to the proposed coherence-scale (green), partly in transition zone (yellow), and some frequencies (red) at decoherent positions; (e) Cytosine, NIST. Remark: Overall pattern is predominantly coherent according to the proposed coherence-scale (green), partly in transition zone (yellow), and some frequencies (red) at decoherent positions.

Valence Band (VB), and the empty Conduction Band (CB). Except that for the high temperature superconductors (HTC), the VB is partially filled, due to Oxygen in the 2D ring layer structure, quite like the CuO plane in HTC ceramics [20] (Figure 4, YBCO). Thus these bio-cells are p type conductors in its normal phase, and would become superconducting at Temperature T below its superconducting transition T_c , yet still within the water phase temperature range [21]. As that happens, the hole states become Bosons with Off Diagonal Long Range Order (ODLRO), with specific binding gap matching to extend the DLRO of the specific eigen-energy monopole bosons within the DNA of the Life form. This induced Long Range symmetry then provides the growth mechanism to the multiplying of the different bio-cells. The genome spectra in the DNA, thereby induce the multiplicity of the different bio-cells in the body. Similarly, the decoherent nitrogenous bases within the DNA causing the genome evolution lead to the death and rebirth with evolution of the bio-cells within the life form. Such evolution is expected to occur in all lives, from viruses to human from generation to the next, hence driving the reproduction of the life form under the survival of the fittest principle. Because of this processes, cancerous growth can also occur. Such cancerous growth can be separated into 2 sources. One that is usually inherited originates from the DNA, while the other caused by the bio-ring and proteins components in the bio-cells structure. Knowledge of these effects can allow for suitable cure approaches.

To investigate this potential cancerous problem, let us start from the formation of RNA and DNA. Note the RNA is a linear chain obtained from the stacking

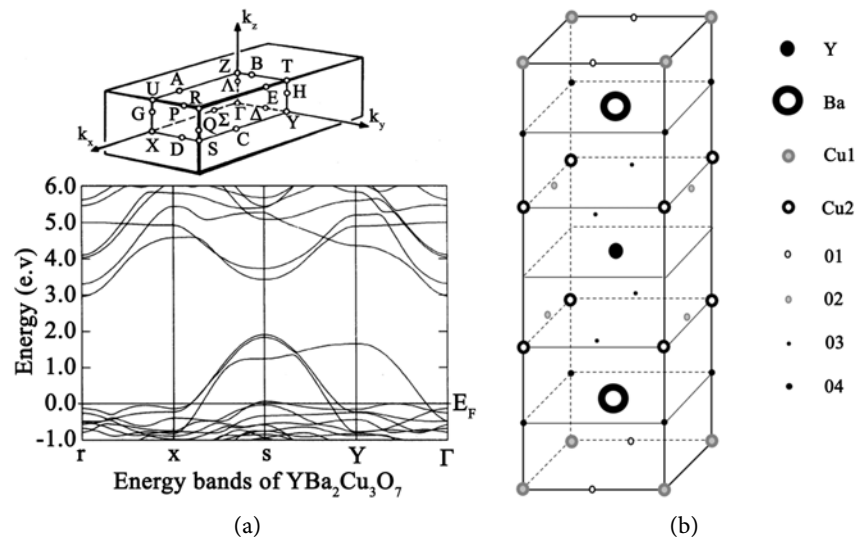


Figure 4. (a) Energy bands of $\text{YBa}_2\text{Cu}_3\text{O}_7$ in the vicinity of the Fermi energy, and the “semiconductor” gap. Inset: The orthorhombic BZ (Wong and Ching, 2004) [20]. (b) The crystal unit cell structure of ceramic superconductor $\text{YBa}_2\text{Cu}_3\text{O}_7$ (Ching *et al.* 1987) [19].

of the 4 nitrogenous bases, linked together due to a backbone built from the chain of Carbon from the N-C-N half of the hexagon of each nitrogenous base. There do not exist an Eigen-monopole state through this backbone, because the DLRO monopole Boson must satisfy the π phase as mentioned in our previous paper [4]. The monopole state can exist by quantum tunneling from one nitrogenous base to the next from the remainder C-C-C in the hexagon. This monopole state however must also obey the rigid end boundary condition of the RNA. Thus it means of the 4 nitrogenous bases, one must act as an end cap. Or more precisely such an end cap base must violate parity symmetry, such that the monopole Boson can only tunnel through one face and not the reverse face. Hence the RNA can only be formed by the random stacking of 7 faces of the 4 nitrogenous bases. This monopole Eigen state then must satisfy the rigid boundary plus the phase matching as it quantum tunnels from each layer to the next adjacent layer. Obviously if the RNA linear chain is twisted due to the backbone twisting, then the phase matching condition is varied and the resulting eigenvalue choice can be infinite.

4. The DNA and RNA Spectra

As mentioned before, there are 7 independent faces from the 4 nitrogenous bases of both the RNA, and DNA from which the monopole DLRO bosons can exist linking the carbon cores within the nitrogenous 3 side by side carbon hexagon, as the backbone spirals, because one nitrogenous base must serve as the end cap. For the RNA, this end cap serves to be the fixed boundary for the boson, while for the DNA, it serves as a reflector such that the boson wave then goes from one RNA side to the other side, making each boson wave completes a close loop. There is no requirement that the intermediate stacking of the 7 faces of the ni-

nitrogenous bases cannot be duplicated, nor can anyone be totally missing. Hence, there are an infinite variety of possible RNAs and DNAs. Only by imposing a no repeat condition can we limit the possibility. In fact, by such an imposition we can get a maximum genome number N of $7! \times 3 \times 2 = 30240$. The factor 3 comes from the 3 side by side carbons tunneling, and the factor 2 comes from the 2 parallel RNAs that make up the DNA. This number is in fact close to that reported for the human genome. That of course does not mean the non-repeat and exact number to be rigorously true for every human. Because each layer of nitrogenous base within the RNA must contain a separation space gap, the two RNAs that make up the DNA, then must be shifted so that they can fit into a tight line. Hence, it also implies these two RNAs can be separated, transforming the DNA structure into a closed ring instead of a line. To get the DNA into a line, it requires the DNA be twisted, by a pair of in-phase spiraling backbones, as shown in **Figure 2**. This 180 degree twisting, then divided the separated nitrogenous bases layers into equal segments of n layers each. Thus resulting in $S = N/n$ segments. Each of these segment Eigen-values of the DLRO bosons performs a special bodily function to inducing the ODLRO of the body cells/organs “p” holes formation, and thus producing the regenerating growth of it.

An error in the nitrogenous bases stacking will result in cancerous growth, and is likely to pass from one generation to the next, the so-called inherited diseases. Recently the biotech firm Intellia Therapeutics announced it is able to edit genes inside the body, based on CRISPR, originally discovered by Jennifer Doudna [22] a 2020 Nobel Prize in Chemistry winner. The method is to zero in the specific segment in the DNA, where the missed nitrogenous base occur that led to the specific organ problem, and just separate that specific segment into a doughnut-like ring, such that the correct nitrogenous base can be replaced and properly installed into the DNA. Intellia studied the specific disease “transthyretin” associated with the liver function, and by just replacing a few DNAs in the liver was shown successful. Of course, not all inherited diseases are as simple as transthyretin, and for how long the disease can be suppressed. Furthermore, direct nitrogenous base replacement can alter the DNA spectra unintentionally leading to unwanted side effects. In fact, the Intellia success in pinpointing the DNA segment where problem lies actually allows for a safer RNA interference (RNAi) approach, letting the body generate the proper DNA itself, such as the methods employed by Alnylam Pharmaceutical [23] and Rocket Pharmaceutical [24].

5. Sensing and Intelligence

The monopole boson states within RNA and DNA that govern the growth and reproduction of bio-cells do not provide animal life forms of its senses, intelligence and accumulation of knowledge. To realize that it is important to recognize that the DLRO monopole bosons require the quantum tunneling ability from within the carbon nuclear void core to the adjacent core. But most chemical elements do not possess a void core similar to carbon 12; for example silicon. Yet

such elements, such as clay are equally created from the Perelmann Ricci-flow entropy mappings, and its molecular weight also obey the Geesink-Jerman-Meijer coherent and decoherent formula [25]. Its conducting electronic states can only be either as free electrons, such as in metals or else as insulators and semi-conductors. Only for metals in the bio-cell structures can it in principle be induced to form an ODLRO superconducting state. It is however well-known through the Bardeen-Cooper-Schrieffer (BCS) [26] theory due to the absence of the exciton mechanism [27], that metallic T_c value is far lower than room temperature, and hence fell out of the DLRO spectra range of the DNAs. In short, there are no electron carriers inducible to create bio-cells. The only activation by the monopole spectra energies is to excite the electron from the filled valence band into the empty conduction band of a coherent semi-conductor bio-molecule, by inducing an electric potential thus making the creation of a computer-like chip circuit possible. These chips circuit existence within an animal allows the animal to build senses, that is sight, sound, smell, taste and pain, plus intelligence as well as memory. Normally this brain center is concentrated in an enclosed bone structure called the head. The charge circuitry feeding the brain is of course still from bio-cells, such as bone marrow, and nerves, which could be cut by blockage at the so-called acupuncture points or become cancerous when we have missed nitrogenous bases within the DNA segments. As well as when the connecting nerve cells die they leave behind the accumulation of dead cells around the brain leading to signal blockage and thereby memory lost, bringing on Alzheimer [28].

6. Conclusion

We have briefly gone through how Life can be created through the topological Perelmann mappings of the homogenous 5D into the non-homogenous Lorentz 4D manifold at room temperature, that is the temperature range of liquid water. And through which coherent and decoherent molecules spectra, including the life-essential elements, water, oxygen and carbon, and clays that then allows for the forming of nitrogenous bases, building up RNA and DNA, so that DLRO monopole bosons spectra can induce the ODLRO of “p” type conducting hole states to create grow of cells and organs, while the clay structures are semi-conductors, and can be organized into computer-like chips, feed by conducting nerves, thus produces senses, intelligence and memory. Each segment of the DNA appears to control the physical function properties of a specific body organ. There are many and complex quantum chemistry, biology and medicine researches already accomplished and many more remain to be found. This over-simplified paper is just an attempt to put everything under a unified mathematical foundation that can be better understood? Hopefully, it can lead to scientifically sound across and combined usage of different known and new successful techniques in the treatment of both yet open inherited and acquired diseases, such as Alzheimer’s.

Acknowledgements

We thank Ms. Winnie So for her tremendous help in the preparation of this

manuscript.

Conflicts of Interest

The authors declare no conflicts of interest regarding the publication of this paper.

References

- [1] Wong, K.W., Dreschhoff, G. and Jungner, H. (2014) The Five Dimension Universe: A Creation and Grand Unified Field Theory Model. Scientific Research Publication, Irvine.
- [2] Aczel, A.D. (1997) Fermat's Last Theorem: Unlocking the Secret of an Ancient Mathematical Problem. Penguin Press, London.
- [3] Maxwell, J.D. (1865) A Dynamic Theory of Electromagnetic Field. *Philosophical Transactions of the Royal Society of London*, **155**, 459-512. <https://doi.org/10.1098/rstl.1865.0008>
- [4] Wong, K.W., Dreschhoff, G., Jungner, H., Fung, P.C.W. and Chow, W.K. (2018) The Magnetic Monopole in 5D Homogeneous Space-Time. *Physics Essays*, **31**, 493-495. <https://doi.org/10.4006/0836-1398-31.4.493>
- [5] Wong, K.W. and Chow, W.K. (2021) A Summary of the Homogeneous 5D Universe Creation Model. Expressed in the Dirac Second-Order Quantization Representation. *Journal of Modern Physics*, **12**, 123-138. <https://doi.org/10.4236/jmp.2021.123012>
- [6] Chow, W.K., Fung, P.C.W. and Wong, K.W. (1985) Bose-Einstein Condensation in Superfluid Helium Four. *Journal of the Physical Society of Japan*, **54**, 4490-4493. <https://doi.org/10.1143/JPSJ.54.4490>
- [7] Higgs, P.W. (1964) Broken Symmetries and the Masses of Gauge Bosons. *Physical Review Letters*, **13**, 508-509. <https://doi.org/10.1103/PhysRevLett.13.508>
- [8] Wong, K.W., Dreschhoff, G.A.M. and Jungner, H.J.N. (2012) The Homogeneous 5D Projection and Realization of Quark and Hadron Masses. arXiv: 1202.5761v1.
- [9] Wong, K.W., Dreschhoff, G. and Jungner, H. (2012) On Neutrino Oscillation and Predicting the 125 GeV Two Photon Emission State from p-p Collision Based on the 5D Homogeneous Space-Time Projection Model. *Journal of Modern Physics*, **3**, 1450-1457. <http://dx.doi.org/10.4236/jmp.2012.310179>
- [10] Wong, K.W., Fung, P. and Chow, W.K. (2019) 5D Model Theory for Creating of Life Forms. *Journal of Modern Physics*, **10**, 1548-1565. <https://doi.org/10.4236/jmp.2019.1013103>
- [11] Schrodinger, E. (1992) What Is Life? Cambridge University Press, New York. <https://doi.org/10.1017/CBO9781139644129>
- [12] Geesink, H.J. and Meijer, D.K.F. (2018) A Semi-Harmonic Frequency Pattern: Organizes Local and Non-Local States by Quantum Entanglement in both EPR-Studies and Life Systems. *Journal of Modern Physics*, **9**, 898-924. <https://doi.org/10.4236/jmp.2018.95056>
- [13] Meijer, D.K.F., Jerman, I., Melkikh A.V. and Sbitrev V.I. (2020) Biophysics of Consciousness: A Scale-Invariant Acoustic Information Code of a Superfluid Quantum Space Guides the Mental Attribute of the Universe. In: Bandyopadhyay, A. and Ray, K., Eds., *Rhythmic Oscillations in Proteins to Human Cognition Book*, Springer/Nature Publisher, Singapore, 213-361.
- [14] Geesink, H.J. (2020) Proposed Informational Code of Bio Molecules and Its Build-

- ing Blocks: Quantum Coherence versus Decoherence. *Private Communication*, preprint.
- [15] Perelman, G. (2002) The Entropy Formula for Ricci Flow and its Geometric Applications. ArXiv.math.DG/0211159.
- [16] Wong, K.W. (1964) Application of Nonlocal Field Operators to a System of Hard Sphere Bose Gas. *Journal of Mathematical Physics*, **5**, 637-642. <https://doi.org/10.1063/1.1704157>
- [17] Perelman, G. (2003) Ricci Flow with Surgery on Three-Manifolds. ArXiv.math.DG-0303109.
- [18] Frohlich, H., (1968) Long-Range Coherence and Energy Storage in Biological Systems. *International Journal of Quantum Chemistry*, **2**, 641-649. <https://doi.org/10.1002/qua.560020505>
- [19] Wong, K.W. and Ching, W.Y. (2004) A Structural-Based Microscopic Theory on High-Temperature Cuprate Superconductors. *Physica C: Superconductivity*, **416**, 47-67. <https://doi.org/10.1016/j.physc.2004.09.003>
- [20] Ching, W.Y., Xu, Y., Zhao, G.-L., Wong, K.W. and Zandiehnam, F. (1987) Electronic Structure and Excitonic-Enhanced Superconducting Mechanism in $\text{YBa}_2\text{Cu}_3\text{O}_{7-\delta}$, *Physical Review Letters*, **59**, 1333-1336. <https://doi.org/10.1103/PhysRevLett.59.1333>
- [21] Wong, K.W. and Curatolo, S. (2008) EEM: The Exciton Enhancement Mechanism Theory and Experimental Evidence of Optically Enhanced T_c in High T_c Superconductors. In: Chang, O.A., Ed., *Progress in Superconductivity Research*, Nova Science Publishers, Inc., Hauppauge, 55-78.
- [22] CNBC (Consumer News and Business Channel) (2021) Intellia Therapeutic CEO John Leonard on Crispr Gene-Editing July 2nd, 2021.
- [23] Yahoo Finance (2021, June 30) Alnylam Initiates KARDIA-1 Phase 2 Study of Zilebesiran (ALN-AGT) in Patients with Mild-to-Moderate Hypertension. <https://finance.yahoo.com/news/alnylam-initiates-kardia-1-phase-110000305.html>
- [24] Yahoo Finance (2021, May 13) Rocket Pharmaceuticals Announces Positive Data from RP-L102, RP-L201 Gene Therapy Programs. <https://finance.yahoo.com/news/rocket-pharmaceuticals-announces-positive-data-160047724.html>
- [25] Geesink, H.J., Jerman, I. and Meijer, D.K.F. (2020) Clay Minerals Information Networking Quantum Coherence Versus Decoherence and First Life. Private Communication.
- [26] Bardeen, J., Cooper, L.N. and Schrieffer, J.R. (1957) Theory of Metallic Superconductivity. *Physical Review*, **108**, 1175-1204. <https://doi.org/10.1103/PhysRev.108.1175>
- [27] Wong, K.W., Fung, P.C.W., Yeung, H.Y. and Kwok, W.Y. (1992) Analysis of Isotope Effect of High T_c Ceramic $\text{YBa}_{2-x}\text{La}_x\text{Cu}_3\text{O}_7$ Using the Excitonic Enhancement Model. *Physical Review B*, **45**, 13017-13024. <https://doi.org/10.1103/PhysRevB.45.13017>
- [28] ABC News (2021, 7 June) New Alzheimer's Drug Is 1st of Its Kind to Be FDA Approved. <https://abcnews.go.com/Health/alzheimers-drug-1st-kind-fda-approved/story?id=78128617>

Inventory of Radiation Protection in Hospitals of Level III in Senegal

Boucar Ndong¹, Sidi Ahmed Dia², Mamadou Salif Djigo¹, Herbert Fachinan³, El Hadji Lamine Bathily¹, Ousseynou Diop¹, Kanta Ka⁴, Gérard Léra Kelvin Akpo⁵, El Hadji Fallou Diouf⁶, Louis Auguinstin Diaga Diouf⁶, Pape Mady Sy⁶, Alphonse Djiboune⁶, Gora Mbaye⁶, Maguette Diagne⁷, Omar Ndoye¹, Mamadou Mbodji¹

¹Laboratoire de Biophysique, Médecine Nucléaire, Université Cheikh Anta Diop, Dakar, Senegal

²Service de Médecine du Travail, Université Cheikh Anta Diop, Dakar, Senegal

³Faculté de Médecine, Université de Parakou, Parakou, Benin

⁴Service de Radiothérapie de Dalal Jamm, Dakar, Senegal

⁵Service de Radiologie de l'Hôpital Aristide Le Dantec, Dakar, Senegal

⁶Laboratoire de Physique Pharmaceutique, Université Cheikh Anta Diop, Dakar, Senegal

⁷Service de Radiothérapie de l'Hôpital Aristide Le Dantec, Dakar, Senegal

Email: ndongboucar73@yahoo.fr

How to cite this paper: Ndong, B., Dia, S.A., Djigo, M.S., Fachinan, H., Bathily, E.H.L., Diop, O., Ka, K., Akpo, G.L.K., Diouf, E.H.F., Diouf, L.A.D., Sy, P.M., Djiboune, A., Mbaye, G., Diagne, M., Ndoye, O. and Mbodji, M. (2021) Inventory of Radiation Protection in Hospitals of Level III in Senegal. *Open Journal of Biophysics*, 11, 397- 406.

<https://doi.org/10.4236/ojbiphy.2021.114016>

Received: September 4, 2021

Accepted: October 26, 2021

Published: October 29, 2021

Copyright © 2021 by author(s) and Scientific Research Publishing Inc. This work is licensed under the Creative Commons Attribution International License (CC BY 4.0).

<http://creativecommons.org/licenses/by/4.0/>



Open Access

Abstract

The aim of this study was to evaluate the level of protection of employees who are exposed to radiation in a level III hospital establishment. It was a descriptive cross-sectional survey of six months' duration, involving eight level III Hospitals (Aristide Le Dantec, Fann, Hoggy, Hear, Abass Ndao, Pikine, Touba, and Thiès) in Senegal. Sixty-one of the one hundred questionnaires were recovered (overall response rate of 61%). The population of the study was mainly female (54.1%). The average age was 38.57 with extremes ranging from 23 to 65 years old. In the places where ionizing radiation sources are handled, only at the Aristide Le Dantec Hospital did we find a "competent person in radiation protection". This explained the lack of a classification of employees and work areas. Forty out of sixty-one (73.77%) had no knowledge of the basic principles of radiation protection (justification, optimisation, dose limitation) and had not ever taken radiation holidays. For radiovigilance, exposure time limits to ionizing radiation concerned only 29/61 or 47.54% of the study population. The inverse square law of distance was known by only 40 workers, of whom 15 had no compliance. We found the presence of dosifilms in only 7/61 or 11.47% of the workers. On the other hand, the use of lead aprons was well established and concerned 57/61 workers, *i.e.*, 93.44%. In sum, ionizing radiation causes adverse health effects. The absence of a good radiation protection culture in Senegal requires the presence of at least 4 to 5 competent persons in radiation protection for quality training of workers in radiobi-

ology, radiopathology and radiation protection.

Keywords

Ionizing Radiation, Radiation Protection, Workers, Senegal

1. Introduction

Ionizing radiation is widely used in the medical field for diagnoses and therapies. In Senegal, we are witnessing the use of increasingly important equipments, standard X-ray machines, computer tomography and linear particle accelerators [1]. SANE *et al.* [2] showed an insufficient level of knowledge of physician in terms of patient radiation protection and an underestimation of radiation-induced cancers that may result from any exposure. Hence the implementation of radiation protection measures for nearly a century. To avoid unnecessary exposure of patients and workers, three main principles such as justification, optimization and dose limitation have been established by international and national organizations [3]. And to respect these principles, radiation protection rules and measures have been defined such as the respect for distance, wearing a lead apron and exposure time. This work will show the level of application of these radiation protection rules and practices in level III health structures in Senegal.

2. Material and Study Method

The study was carried out in eight medical imaging departments of level III hospitals, six of which were in the capital (Aristide de Ledantec, Fann, Hôpital Général Idrissa Pouye, Albert Royer, Abass Ndao, Pikine), one in the Thiès region (Thiès hospital) and one in the Diourbel region (Fawzaini hospital). This was a prospective cross-sectional study lasting six months. A questionnaire was sent to the highest authority in the hospital before being distributed to the target group, which included radiologists, doctors in training, medical imaging technicians, assistant technicians, stretcher bearers, secretaries and other administrative staff. Several parameters were of interest to us in the course of the study, namely demographic data, radiation source, exposure time, zoning, compliance with the radiation holiday, worker classification and individual radiation protection equipment (wearing of dosifilm, lead apron, glasses, etc.).

3. Results

3.1. Socio-Demographic Aspects

Sixty-one of the 100 forms (61%) were completed. The female sex participating in the survey was largely dominant (85/100). The average age of the workers was 38.57 years, with extremes of 23 and 60 years. The modal age was 40 years and the median age was 37.5 years. The table below (**Table 1**) represents the distribution of workers.

Table 1. Distribution of workers according to their place of work.

Hospital structures	Workforce	Percentage (%)
HEAR	01	1.64
CHAN	10	16.9
CHFANN	11	18.03
HALD	21	34.83
HOGGY	06	09.84
FAWZAINI	03	04.92
PIKINE	05	08.20
THIES	04	06.56

Figure 1 shows the different proportions of socio-professional categories.

Figure 2 shows the distribution of employees according to seniority.

3.2. Regulatory Framework

Of the eight hospitals, with the exception of the radiotherapy department of the Aristide de Le dantec hospital, none had a competent person in charge of radiation protection (PCR).

With regard to workers' knowledge of the regulations, forty-five workers (73.77%) had no knowledge of the regulations. This lack of knowledge of the texts largely concerned assistant technicians in most cases (9/10), followed by doctors (5/10), technicians (3/10) and an almost total lack of knowledge of these texts by secretaries, stretcher-bearers and the other components. These workers have no knowledge of the texts.

As for workers' radiological leave, three quarters (75%) have never had any leave related to ionizing radiation.

3.3. Exposure Parameters

➤ Sources of exposure

The X-ray tube was the main source of exposure to ionizing radiation in the eight hospitals.

➤ Modality of medical imaging examination

During the study period, several types of medical imaging examinations were performed. **Table 2** presents the modalities of medical imaging examinations performed by the employees.

➤ Duration of daily exposure

The duration of daily exposure to ionizing radiation varied from one centre to another and from one occupational category to another during our study. It varied from two hours to more than eight hours. **Table 3** shows the distribution of the average daily exposure time by category of employee.

➤ Workplace layout and zoning

None of the facilities surveyed had a posted floor plan or zoning according to their level of exposure.

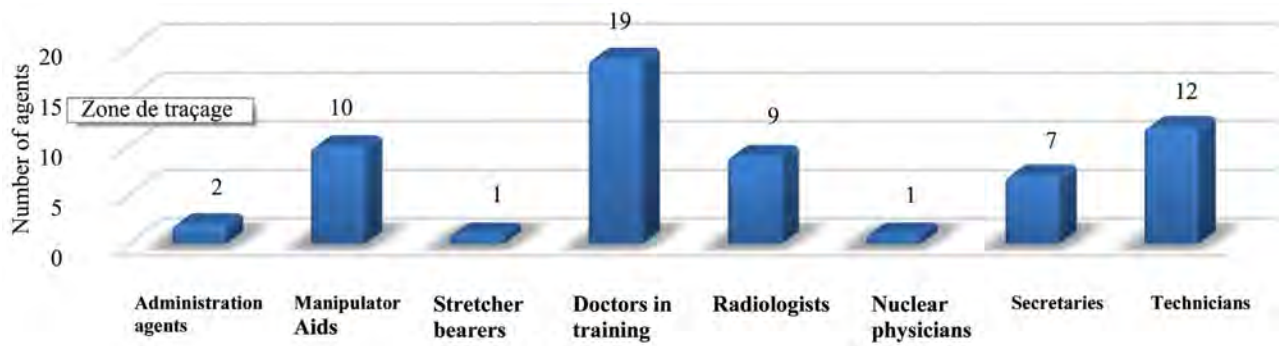


Figure 1. Distribution of surveyed staff in medical imaging departments according to socio-professional category.

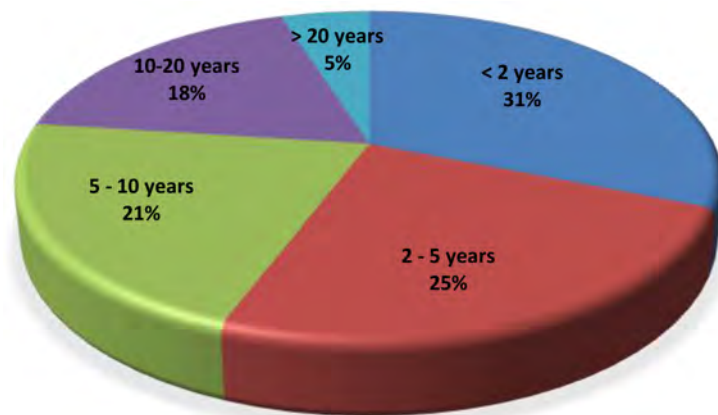


Figure 2. Distribution of employees according to seniority.

Table 2. Modalities of medical imaging examinations carried out by the employees.

Examination modality	Number of employees
Dental panorama	1
Conventional radiography	55
Mammography	44
Computed tomography	43
Interventional radiology	1
Scintigraphy	1

Table 3. Distribution of the average daily duration of exposure by category of employee.

Average exposure time	Category of employees						Total	Percentage (%)
	Handling assistants	Technicians	Medical doctors	Secretaries	Other			
2 hours	0	0	1	0	0	1	1.64	
4 hours	0	0	8	0	0	8	13.11	
6 hours	3	3	12	1	1	21	34.83	
8 hours	3	7	7	5	1	23	37.71	
More than 8 hours	4	1	1	1	1	8	13.11	

3.4. Radiological, Dosimetric and Medical Monitoring

No radiological monitoring was carried out in the hospitals studied.

The use of passive dosimeters worn on the chest was observed only in seven workers exposed to ionizing radiation, *i.e.*, 11.47% of workers. The dosimeters were collected quarterly and processed in France in approved institutes.

None of the health facilities subjected the staff to a medical examination (at the time of hiring, periodically and when returning to work) or to additional radio monitoring examinations (CBC, chest X-ray, ophthalmological, dermatological and ENT examinations). No worker exposed to ionizing radiation had a medical file containing the regulatory information.

3.5. Compliance with Radiation Protection Measures

➤ Reduction of exposure time

The daily time spent in the medical imaging room ranged from two hours to over eight hours.

Due to work constraints, thirty workers (49.18%) remained in the room while the X-ray tube was active.

Eight workers (13.11%) were in the room outside of work constraints while the X-ray tube was inadvertently activated due to the absence of light signals. In addition, twenty-nine (29) workers had not reduced their exposure time, *i.e.* 47.54% of the workers.

Nine doctors, *i.e.*, one third of their workforce, had not alternated their shifts, five radiology technicians (41.66%) and six assistant radiographers had not done so either.

➤ Distance from the Source

Fifteen workers, or 24.6% of the workforce in the imaging departments, did not concern themselves with the regulatory distance from the source of ionizing radiation.

➤ Interposition of protective screens

The plumber's apron was the most commonly used personal protective equipment. Fifty-seven workers under ionizing radiation, *i.e.* 93.44%, wore personal protective equipment if the situation required it. **Figure 3** shows the distribution of the wearing of personal protective equipment by category of worker.

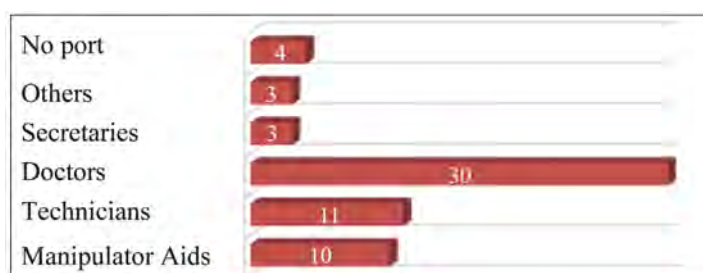


Figure 3. Distribution of the wearing of personal protective equipment by category of worker.

4. Discussion

4.1. Socio-Demographic Aspects

The staffs in the radiology departments of level III hospitals are relatively young, with an average age of 37.5 years. The majority of these staffs are female, with an estimated ratio of women to men of 0.85. As a result, there should be special monitoring of radiation protection as there are a significant number of individuals of childbearing age in this population. Thus, any pregnancy should be reported to the occupational physician for appropriate management in the absence of PCR observed in most medical imaging departments [4]. The young nature of the population studied is another reason to tighten up radiation protection measures, as Bergonié Tribondeau's law of 1906 specifies that the cells of young subjects, which multiply rapidly, are the most radiosensitive, unlike the well-differentiated cells of older subjects, which are not very radiosensitive in principle.

4.2. Regulatory Framework and Presence of a Competent Person in Radiation Protection

The rules of radiation protection are not country-specific, but result from guidelines provided worldwide. Standards or recommendations are established at international level by different organizations. The International Atomic Energy Agency (IAEA) publishes and regularly revises standards in the fields of nuclear safety and radiation protection based on ICRP recommendations [4].

In Senegal, the organization of radiation protection is governed by three fundamental texts that define the general principles and establish the legal means for their actions [5]. Efficient control of nuclear activities to ensure the protection of workers, the environment and patients against ionizing radiation is accompanied by penal sanctions in case of infringement of this legislation [5]. In our study, the lack of knowledge of the regulations among most of our study population is largely explained by the absence of a PCR. A similar observation was made by Jaouad in Morocco in a study on the radiation protection of workers in Morocco. He noted in 2013 that 43% of his study population was unaware of the texts governing radiation protection due to the absence of a PCR in most imaging centres [6]. And this lack of PCRs is found almost everywhere. Indeed, Kouassi *et al.* in 2005 observed the presence of a PCR in 16.67% of the facilities surveyed in Abidjan in Côte d'Ivoire [7]. Tapsoba *et al.* in 2010 found that only 5.9% of radiology departments in Ouagadougou in Burkina Faso had a PCR [8]. However, studies carried out by Khaled *et al.* in 2010 found a high frequency of PCR with 50% of imaging centres having it. Thus, Sidi Bel-Abbés in Algeria [9] found a clear culture of radiation protection among these workers, contrary to what happens in West Africa and particularly in Senegal. Indeed, the PCR ensures the implementation of radiation protection measures. She is responsible and specially trained, with a knowledge check every five years. This implementation is based on regulatory texts that define in particular the controls of personnel, premises and ionizing radiation sources. This PCR implements all the ne-

cessary measures to reduce exposures as little as possible in order to achieve a resolved image or effective treatment. It is this person who organizes the dosimetric monitoring of category A and B personnel, controls the ambient exposure rate, searches for contamination, and monitors the entry and exit of ionizing radiation and the storage of radioelements in nuclear medicine. It also provides staff training and enables the dissemination of a “radiation protection culture” which requires unflinching vigilance and rigorous working conditions.

4.3. Exposure Parameters

The sources of hospital exposure to ionizing radiation in our series were largely dominated by conventional radiography and CT scanning. Maintenance and quality control of the equipment is necessary as these defects accentuate the production of scattered radiation which results in unnecessary irradiation of patients and the production of poor resolution images. In our developing countries, the maintenance of radiology equipment is precarious and a certain number of machines are obsolete with an operating life of more than 10 years. This was confirmed by Kouassi *et al.* in a study carried out in Ivory Coast in 2005 where they found that 61.5% of the equipment had been in use for more than ten years [7].

In this study, the average duration of exposure varied according to the facilities. Indeed, the daily exposure mode is about eight hours. This poses a real problem, as we know that the longer the exposure time, the more likely it is that stochastic effects will lead to genetic effects and cancer.

Other medical imaging modalities that do not use ionizing radiation, such as ultrasound and magnetic resonance imaging, provide an alternative way of managing the duration of exposure to radiogenic sources.

4.4. Medical and Dosimetric Monitoring

The absence of a health structure for monitoring workers who were not able to benefit from a single chest X-ray examination during their recruitment and were not monitored periodically. This follow-up should allow early detection of pre-cancerous lesions and the organization of therapeutic and medico-legal management of radiation-induced pathologies. Mbo Amvene *et al.* made the same observation in the imaging departments of hospitals in the far north of Cameroon in 2017. The same is true for Houndétoungan in hospitals in south-eastern Benin in 2015 [10] [11].

As for dosimetric monitoring, only 11.47% of workers had benefited from it. And yet, all workers exposed to ionizing radiation must have medical and dosimetric monitoring. Depending on their activity and level of exposure, this may be a passive or active dosimeter. The accumulation of the doses received helps the occupational physician to anticipate the occurrence of radiation-induced pathologies. To avoid this situation, biological examinations such as blood counts should be carried out on these workers, as it has been clearly established by authors

such as Jimonet *et al.* in 2007 that even low-dose exposures are likely to have harmful effects on workers [12].

4.5. Compliance with Radiation Protection Measures

The practical implementation of radiation protection measures is mainly based on the interposition of protective shields, the distance from the source and the reduction of the exposure time.

➤ Interposition of protective screens

The plumber's apron is the most commonly used personal protective equipment. Fifty-seven workers under ionizing radiation, *i.e.* 93.44%, often wear personal protective equipment if the situation requires it. Studies on compliance with radiation protection measures in other African countries with national regulations have also shown an acceptable level of compliance with regard to the wearing of aprons. Indeed, Kouassi *et al.* in Abidjan in 2005 [7] and Tapsoba *et al.* in Ouagadougou [8] had reported that more than 90% of workers protected themselves with a lead apron. Jaouad noted this in 80% of his respondents in 2013 in Marrakech [6]. In contrast, Khaled found a proportion of 50% use of plumber's aprons by workers in his 2010 study in the health care facilities of the city of Sidi Bel-Abbés [9]. The lack of regular wearing of lead aprons is indicative of the lack of rigor of the staff with regard to their own protection. It was considered as "a waste of time" for the performance of an examination or simply "useless because the screen protects enough" according to some workers. The other reason most mentioned was its heaviness. However, according to Menechal *et al.* certain types of apron are more easily used and well tolerated because they are more adapted to the worker's morphology and lighter [13].

As for the other protective equipment (thyroid protectors, goggles, leaded gloves), they were almost never used in the departments that had them. Kouassi *et al.* [7] in Abidjan made the same observation, while in Marrakech, Jaouad found that only 17.9% of workers used them [6].

➤ Reduction of exposure time

The daily time spent in the medical imaging room ranged from 2 hours to more than 8 hours. For work-related constraints, thirty workers (49.18%) remained in the room while the X-ray tube was active.

Eight workers (13.11%) were in the room outside of work constraints while the X-ray tube was inadvertently activated due to the absence of light signals. This malfunction increases the exposure time of the workers with an additional accumulation of absorbed dose.

Administrative measures such as technical leave, alternating shifts are not applied for all categories of workers. Forty-five workers interviewed had never benefited from radiation leave (73.77%). Assistant technicians and doctors in training, who do not have administrative status, constitute the largest number of workers and do not have radius leave. Khaled *et al.* found in their study in Algeria in 2010 that only 20% of workers benefited from it [9].

The involvement of the administrative authorities of the hospital structures, the Ministry of Health, the Ministry of Employment and Labour and the authorities of the medical imaging department is necessary for the proper harmonization of these leaves, which will substantially promote the reduction of workers' exposure time to ionizing radiation.

➤ Distance from the Source

Fifteen workers, or 24.60% of the imaging staff, were not concerned about the regulatory distance from the ionizing radiation source. Staff should, at all times, keep as far away as possible from the source of ionizing radiation. Personnel should never be allowed direct exposure to the primary radiation beam [14].

It is therefore important to comply with building standards, to carry out a good zoning of the premises and to regularly carry out a good study of the workstation to ensure optimal protection of the worker [15]. This is difficult to achieve in the absence of a PCR.

5. Conclusion

In Senegal, level III health structure has the most qualified medical staff and despite everything, this study still shows an embryonic state of radiation protection for workers, even fewer patients subjected to ionizing radiation for diagnostic and therapeutic purposes. This is clearly explained by the absence of Qualified Expert in Radioprotection (QER) in most of our departments. The QEC plays a key role. Indeed, it carries out the technical expertise (job study) allowing the classification of radiology rooms by the employer ("zoning"). It ensures that these areas are properly marked and sets up ambient dosimetry. She takes care of dosimetric monitoring requests. It also allows the collection and dispatch of passive dosimeters and at the same time intervenes in the management, prevention and training of newly assigned personnel on the specifics of the service. To give an important place to radiation protection, quality control of radiology equipments is needed to optimize the doses delivered to patients. That will instill in workers a real "radiation protection culture".

Conflicts of Interest

The authors declare that they have no conflicts of interest.

References

- [1] Arrivé, L. (2012) Modalités Radiologiques. In: Miquel, A. and Monnier-Cholley, L., Eds., *Imagerie Médicale Pour le Clinicien*, Elsevier Masson, Paris, 1-38. <https://doi.org/10.1016/B978-2-294-71238-8.00001-1>
- [2] Gervaise, A., Esperabe-Vignau, F., Pernin, M., Naulet, P., Portron, Y. and Lapierre-Combes, M. (2011) Évaluation des connaissances des prescripteurs de scanners en matière de radioprotection des patients. *Journal de Radiologie*, **92**, 681-687.
- [3] Nénot, J.C., Brenot, J., Laurier, D., Rannou, A. and Thierry, D. (2007) Recommandations 2007 de la Commission internationale de protection radiologique. ICRP Publication, New Delhi.

- [4] Aurengo, A., Petitclerc, T. and Kas, A. (2013) Biophysique. 4th Edition, Lavoisier SAS, Paris.
- [5] Gouvernement du Sénégal (2004) LOI n° 2004-17 du 15 juin 2004 abrogeant les dispositions de la loi n° 2001-01 du 3 janvier 2001 relative à la protection contre les rayonnements ionisants. *Journal Officiel du Sénégal*, n° 6177.
- [6] Jaouad, S. (2013) Étude de l'observance des règles de la radioprotection en radiologie conventionnelle dans les hôpitaux SEGMA de la Région Marrakech Tensift al Haouz.
- [7] Kouassi, Y.M., Wognin, S.B., Tchicaya, A.F., Alla, D. and Bonny, J.S. (2005) Étude de l'observance des règles de radioprotection en milieu hospitalier à Abidjan. *Archives des Maladies Professionnelles et de l'Environnement*, **66**, 369-374.
[https://doi.org/10.1016/S1775-8785\(05\)79108-6](https://doi.org/10.1016/S1775-8785(05)79108-6)
- [8] Tapsoba, T., Ouattara, T., Belemlilga, H.G.L., Sanon, H., Bamouni, Y.A., Ouédraogo, V., et al. (2010) Application des règles de protection contre les rayons X dans les services de radiologie de Ouagadougou. *Médecine Nucléaire*, **34**, e9-e12.
<https://doi.org/10.1016/j.mednuc.2010.07.011>
- [9] Khaled, A., Ghomari, O. and Kandouci, A.B. (2010) La radioprotection dans les établissements de soins utilisant les rayons X: évaluation et constats dans la ville de Sidi Bel-Abbès. Sidi Bel-Abbès, Algérie.
- [10] Amvene, J.M., Djonyang, B., Amougou, J.M., Ngaroua, D. and Amvene, S.N. (2017) Observance des Règles de Radioprotection dans les Services d'Imagerie des Hôpitaux de l'Extrême-Nord du Cameroun. *Health Sciences and Disease*, **18**, 83-87.
- [11] Houndetoungan, G.D. (2015) Evaluation de l'observance des mesures de radioprotection des travailleurs dans les services de radiologie de l'ouémé et du plateau au Bénin en 2015 [Mémoire de DES, Biologie médicale et sciences fondamentales, Biophysique]. Faculté des Sciences de la Santé de Cotonou.
- [12] Vaillant, L. and Schneider, T. (2012) Evaluation du détriment associé à l'exposition aux faibles doses et faibles débits de dose dans le système de radioprotection. *Environnement, Risques & Santé*, **11**, 149-159.
- [13] Menechal, P., Valero, M., Megnigbeto, C., Marchal, C. and Godet, J.L. (2011) La radioprotection des patients et des travailleurs en radiologie interventionnelle et au bloc opératoire. *INRS (Institut National de Recherche et de Sécurité)*, **222**, 27-33.
- [14] Association Française de Normalisation (2011) Normes Française de Construction (NFC). 15-160.
- [15] Cordoliani, Y.S. and Foehrenbach, H. (2014) Radioprotection en milieu médical: principes et mise en pratique. 3rd Edition, Elsevier Masson, Paris, 230.

ROC and SAT Analysis of Different Grayscale Test Images (Distractors L and Target T) to Customize a Visual-Search Attention Task

Dineshen Chuckravanen*, Barkin Ilhan, Nizamettin Dalkılıç

Department of Biophysics, Meram Faculty of Medicine, Necmettin Erbakan University, Konya, Turkey

Email: *dineshen2013@gmail.com

How to cite this paper: Chuckravanen, D., Ilhan, B. and Dalkılıç, N. (2021) ROC and SAT Analysis of Different Grayscale Test Images (Distractors L and Target T) to Customize a Visual-Search Attention Task. *Open Journal of Biophysics*, 11, 407-414.
<https://doi.org/10.4236/ojbiphy.2021.114017>

Received: May 8, 2021

Accepted: October 26, 2021

Published: October 29, 2021

Copyright © 2021 by author(s) and Scientific Research Publishing Inc. This work is licensed under the Creative Commons Attribution International License (CC BY 4.0).

<http://creativecommons.org/licenses/by/4.0/>



Open Access

Abstract

Nowadays, there is a great need to investigate the effects of fatigue on physical as well as mental performance. The issues that are generally associated with extreme fatigue are that one can easily lose one's focus while performing any particular activity whether it is physical or mental and this decreases one's motivation to complete the task at hand efficiently and successfully. In the same line of thought, myriads of research studies posited the negative effects of fatigue on mental performance, and most techniques to induce fatigue to require normally long-time and repetitive visual search tasks. In this study, a visual search algorithm task was devised and customized using performance measures such as d' (**d-prime**) and Speed Accuracy Trade-Off (**SATF**) as well as **ROC** analysis for classifier performance. The visual search algorithm consisted of distractors (**L**) and a target (**T**) whereby human participants had to press the appropriate keyboard button as fast as possible if they notice a target or not upon presentation of a visual stimulus. It was administered to human participants under laboratory conditions, and the reaction times, as well as accuracy of the participants, were monitored. It was found that the test image Size35Int255 was the best image to be used in terms of sensitivity and AUC (Area under Curve). Therefore, ongoing researches can use these findings to create their visual stimuli in such a way that the target and distractor images follow the size and intensity characteristics as found in this research.

Keywords

AUC, Mental Fatigue, Psychophysics, ROC Analysis, Response Accuracy, Reaction Time, SATF, Visual Attention

1. Introduction

Fatigue is defined as a condition or phenomenon of decreased ability and effi-

ciency of mental and/or physical activities caused by excessive mental and/or physical activities, or illness. It is characterized by decreased energy, motivation and difficult concentrating or difficulty in maintaining sustained attention and remaining alert to relevant stimuli appearing at unpredictable time points over long periods of time. Fatigue is usually accompanied by a sense of discomfort, desire to rest and reduced motivation [1]. There are many types of different works such as driving, monitoring tasks which require operators to maintain sustained attention on multiple objects for prolonged periods of time. One of the principal causes of decrements in sustained attention is mental fatigue [2] which was defined as the state of reduced mental alertness that impairs performance. There are many studies which showed the adverse effects of mental fatigue on sustained attention as shown by reduced behavioural performance. For instance, in sustained attention to response task [3] found that participants' performance declined in both accuracy and speed in time. It was found that as the duration of the mental fatiguing induced task increases, the number of misses and false alarms increase, and the response speed decreases [4]. In these studies as well as those from research [5], participants were instructed to execute a task continuously for a long period of time, and then their behavioural performances, reactions times and accuracy rates, were compared between the former and the latter of the mental fatigue induced experiment [6]. Moreover, factors that can induce fatigue in a short period of time can be a very boring/monotonous task, a bad/dark illuminating, night time, combination with physical fatigue and low-performance phases according to circadian rhythm.

To date, in most fatigue studies, the methods used to induce fatigue are either through sleep deprivation or the performance of long-term, tedious and repetitive tasks. Moreover, there are many researches study which employ and support long-time repetitive visual search tasks to induce mental fatigue [7]. For instance, authors [7] [8] used a visual search task to induce mental fatigue and they found promising electroencephalogram indicators for mental fatigue and evaluation. Moreover, researchers [9] found that visual search is a promising instrument for the assessment of cognitive functions and cognitive changes in patients with multiple sclerosis because of its good discriminatory power and insusceptibility to practice effects. Therefore, this research developed and attempted to customize a visual search algorithm task which consisted of distractors and a target.

2. Methodology

The visual search algorithm was developed using GNU Octave programming language running on Linux (Debian8). The visual search algorithm displays a number of rotated distractors (L) and a rotated target (T) presented randomly on a Cathode Ray Tube (CRT) monitor's screen with width 600 and height 480. The number of distractors including the target (N) was varied from 12 to 28 in increments of 4. The image size of the distractor L and that of the target T were varied from [25 × 25] pixels to [40 × 40] pixels in increments of 5 to produce 4

different image sizes. Then, the image intensity for each particular distractor image size as well as the target image size was varied in the following manner: 220, 230, 240 and 255. This produces in total 16 types of grayscale test images for the distractor L and 16 types of grayscale test images for the target T. Some examples of the images are shown in **Figures 1-3**. The distance between the participants and the monitor screen was kept at constant at 60 cm.

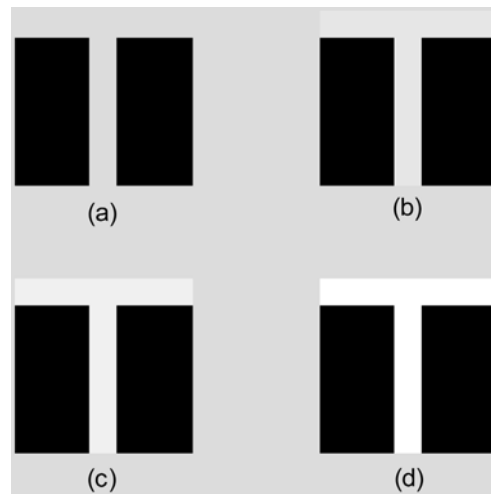


Figure 1. Displays target T of size 40×40 pixels in different intensity of 220, 230, 240 and 255. (a) Size 40Int220; (b) Size 40Int230; (c) Size 40Int240; (d) Size40Int255.



Figure 2. Test image of target T at different image size in respective size [Pixel \times Pixel]. (a) 40×40 ; (b) 35×35 ; (c) 30×30 ; (d) 25×25 .

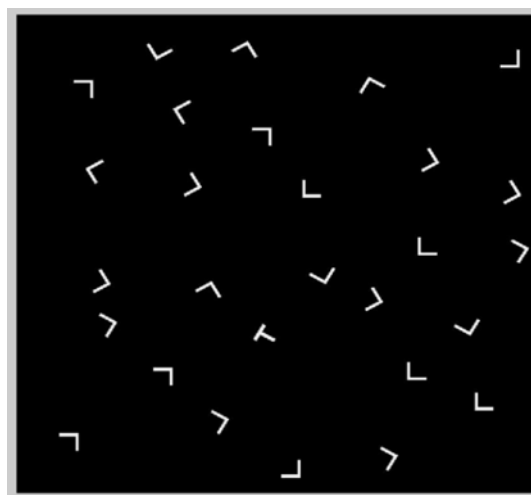


Figure 3. A screenshot of the visual search task with a random set size of 28 including the target and distractors. The distractors as well as the target are randomly rotated throughout and spread across the screen.

2.1. Participant Recruitment

The whole research study ethics was approved by Tubitak's Ethics committee. Prior to performing the visual search task, an informed consent form was provided to each participant to demonstrate their willingness to take part in this psychophysics experiment. The psychophysics experiment took about 20 minutes, and each participant was required to press the right-arrow key on the keyboard when he or she sees a target T among randomly shown distractors L on the screen or to press the left-arrow key on the keyboard when he or she do not see a target T among randomly shown distractors L on the screen. The participants were required to press the appropriate key as quickly and accurately as possible. Participants could withdraw from the experiment at any time while performing the psychophysics experiment if they did not feel comfortable to continue, and their results were eventually withdrawn from the recorded database. All participants' responses data were coded and no names were be divulged during this dissemination. A total number of 18 participants took part in this study of which 10 were males and 8 were females. The healthy participants comprised of medical students of different years of study (1st year to 6th year of their medical studies), and also research staff of the biophysics, physiology and biology department of Necmettin Erbakan University. Their ages range from 19 to 51 years old (24.8 ± 8.2).

2.2. Data Collection

Both reaction times (response times) as well as the responses of the participants were recorded. The responses of the participants were compared to the presence or absence of target in a particular screen. Moreover, the different set sizes of the number of distractors including target for each screen were recorded.

2.3. ROC Analysis

A Receiver Operating Characteristics (ROC) graph is a technique for visualizing, organizing and selecting classifiers based on their performance. ROC graphs have been employed in signal detection theory to depict the tradeoff between hit rates and false alarm rates of classifiers. ROC analysis has been extended for use in visualizing and also analyzing the behavior of diagnostic systems. One of the earliest adopters of ROC graphs in machine learning was Spackman (1989), who demonstrated the value of ROC curves in evaluating and comparing algorithms.

Classifier Performance

A classification model or classifier is a mapping from instances to predicted classes. Given a classifier and an instance, there are four possible outcomes. If the instance is positive, and it is classified as positive, it is counted as a true positive; if it is classified as negative, it is counted as a false negative. If the instance is negative and it is classified as negative, it is counted as true negative; if it is classified as positive, it is counted as a false positive. Given a classifier and a set of instances (the test set), the following terms are defined [10] [11]:

The true positive rate (also called the hit rate and recall) is estimated as:

1) Tp -rate = positives correctly classified/total positives

The false positive rate (also called the false alarm rate) of the classifier is:

2) Fp -rate = Negatives incorrectly classified/Total negatives

Other terms derived from these two rates are:

3) Specificity = $1 - fp$ rate

Specificity measures the proportion of negatives that are correctly identified.

4) Sensitivity = tp rate

Sensitivity measures the proportion of positives that are correctly identified.

In this research, the Receiver Operator Characteristics (ROC) analysis was applied to the reaction times of the participants that were affected by the different image size and image intensity as well as the number of distractors on a particular screen. In this psychophysics experiment, for each participant, the target was present at 50% of the screen presentations in order to observe how well the reaction times could be used to predict the two different classes of presence of target on a screen and the absence of target on a particular screen. The Area under Curve (AUC) of an ROC curve will pinpoint the best test image(s) for this particular visual task in terms of specificity and sensitivity.

2.4. SAT Analysis

There is normally a negative relationship between reaction times and accuracy of responses. It means that the faster one reacts in a particular task, the worse is one's performance (accuracy). The confusion matrix summarizes the different types of true positives, false positives, true negatives as well as false negative that might occur during an experiment (**Table 1**). Therefore, for the Speed Accuracy trade-off analysis, the ratio of d-prime (d') or sensitivity index to reaction time was investigated for each test image and it is also called as the Speed-Accuracy Tradeoff Function (SATF). The d' (d-prime) is a statistic used in signal detection theory and it provides the separation between the means of the signal and the noise distributions, compared against the standard deviation of the signal or noise distribution. An estimate of the d' can be found from the measurement of the hit rate and the false alarm rate based on the confusion matrix (**Table 1**). It is calculated as $d' = Z(\text{hit rate}) - Z(\text{false alarm rate})$ where function $Z(p)$, $p \in [0, 1]$, is the inverse of the cumulative distribution function of the Gaussian distribution. A higher d' indicates that the signal can be more readily detected.

Table 1. Confusion matrix to describe the target present and target absent responses to differentiate between true positive, false positive, false negative and true negative.

	Target present (P)	Target absent (N)
Response (Yes)	True positives	False positives
Response (No)	False negatives	True negatives

Based on the SATF function, low constant d' for low reaction times mean the Task is too difficult and if high constant d' for high reaction time, this means performance saturates.

3. Results

A detailed summary of the results produced from the ROC analysis, d' , the mean reaction times of the participants for each test image as well as the corresponding responses' accuracy are shown in **Table 2**. The percentage accuracy of the responses is computed by dividing the number of correct responses with the total number of questions posed to the participants. The reaction times of the participants' responses are classified using ROC technique (see **Figure 4**).

SATF analysis was conducted on the test image Size35Int255 based on its high d' and highest AUC values to observe the change in sensitivity with increasing reaction times of the participants (see **Figure 5**).

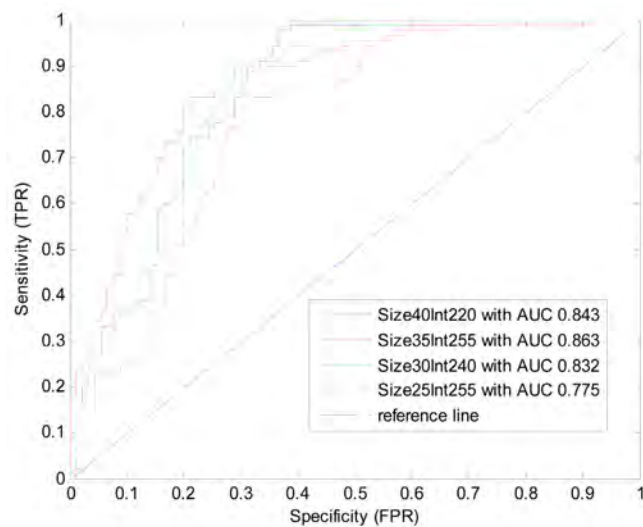


Figure 4. ROC analysis of reaction times of the participants in successfully being classified in two classes (screen with target and screen without target) to display the behaviour of the selected test images. The reference line shows an imaginary line that divides the graph into equal percentages (50%).

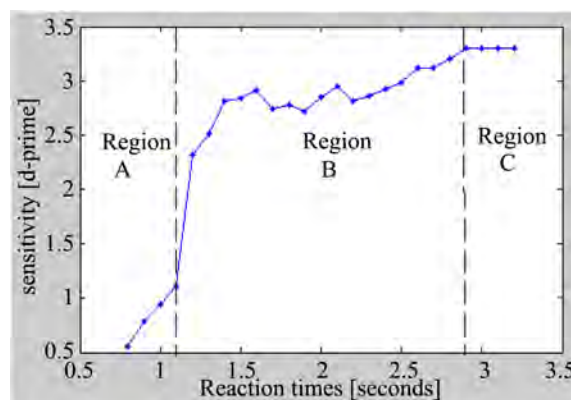


Figure 5. The SATF shows how the sensitivity changes with increasing reaction times.

Table 2. ROC analysis, dprime, mean RT and accuracy.

Test images	Area under curve from ROC analysis	Dprime [d' = z(H) – z(F)]	Mean reaction time (s)	Percentage accuracy (%)
Size40Int255	0.7810	1.683	1.642	90.0
Size40Int240	0.8574	3.002	1.984	96.1
Size40Int230	0.8441	3.002	1.964	96.7
Size40Int220	0.8430	3.184	1.842	97.2
Size35Int255	0.8631	3.403	1.894	96.1
Size35Int240	0.8220	2.840	1.922	96.1
Size35Int230	0.7996	3.667	2.090	98.3
Size35Int220	0.8344	3.186	1.962	96.7
Size30Int255	0.8491	3.002	2.059	95.6
Size30Int240	0.8321	2.328	1.989	92.7
Size30Int230	0.8094	3.668	2.019	98.3
Size30Int220	0.8275	2.693	2.012	95.6
Size25Int255	0.7775	2.327	2.292	93.3
Size25Int240	0.8270	2.441	2.241	91.7
Size25Int230	0.7967	2.441	2.244	94.4
Size25Int220	0.8311	2.121	2.084	92.7

4. Discussion and Conclusion

ROC analysis proved to be a useful tool in distinguishing the effect of the different types of images (distractors and targets) on the subjects' reaction times. The highest value of AUC was the test image with size of 35×35 pixels and with an image intensity of 255 and it represented the best test image in terms of specificity and sensitivity. Moreover, the results based on the d-prime alone showed that the test image Size35Int255 ranked among the first three best images to represent a readily detected visual stimulus. Speed-accuracy trade-off function analysis on the test image Size35Int255 showed that the sensitivity increases sharply between the reaction times of 0.8 to 1.1 seconds, then sensitivity rises gradually until 2.8 seconds and then sensitivity remains constant beyond this point which insinuates that performance saturates at this point onward. The ongoing analysis is also focusing on the effect of a varied number of targets and distractors on the participants' performance.

Acknowledgements

This research work is supported by The Scientific and Technological Research Council of Turkey (TÜBİTAK) and the Marie Curie Action Cofund of the 7th Framework Program (FP7) for me to pursue my postdoctoral research work. I would like to sincerely thank the medical students as well as the various research staffs from the Biophysics, Biology and Physiology Departments of the Necmet-

tin Erbakan University for their precious participation as well as for helping me in the organization (scheduling and translation) process of this psychophysics experiment. My sincere thanks go also to my mentors Assoc. Professor Barkin Ilhan for his fruitful advice and guidance about performance algorithms, and the concept of the rotation of the targets and distractors, and Prof. Nizamettin Dalkılıç about the support of this work.

Conflicts of Interest

The authors declare no conflicts of interest regarding the publication of this paper.

References

- [1] Altman, D.G. and Bland, J.M. (1994) Statistics Notes: Diagnostic Tests 1: Sensitivity and Specificity. *British Medical Journal*, **308**, Article No. 1552. <https://doi.org/10.1136/bmj.308.6943.1552>
- [2] Qian, S., Li, M., Li, G., Liu, K., Li, B., Jiang, Q., *et al.* (2015) Environmental Heat Stress Enhances Mental Fatigue during Sustained Attention Task Performing: Evidence from an ASL Perfusion Study. *Behavioural Brain Research*, **280**, 6-15. <https://doi.org/10.1016/j.bbr.2014.11.036>
- [3] Bonnefond, A., Doignon-Camus, N., Touzalin-Chretien, P. and Dufour, A. (2010) Vigilance and Intrinsic Maintenance of Alert State: An ERP Study. *Behavioural Brain Research*, **211**, 185-190. <https://doi.org/10.1016/j.bbr.2010.03.030>
- [4] Boksem, M.A., Meijman, T.F. and Lorist, M.M. (2005) Effects of Mental Fatigue on Attention: An ERP Study. *Cognitive Brain Research*, **25**, 107-116. <https://doi.org/10.1016/j.cogbrainres.2005.04.011>
- [5] Kato, Y., Endo, H. and Kizuka, T. (2009) Mental Fatigue and Impaired Response Processes: Event-Related Brain Potentials in a Go/No Go Task. *International Journal of Psychophysiology*, **72**, 204-211. <https://doi.org/10.1016/j.ijpsycho.2008.12.008>
- [6] Guo, Z., Chen, R., Zhang, K., Pan, Y. and Wu, J. (2016) The Impairing Effect of Mental Fatigue on Visual Sustained Attention under Monotonous Multi-Object Visual Attention Task in Long Durations: An Event-Related Potential Based Study. *PLoS ONE*, **11**, e0163360. <https://doi.org/10.1371/journal.pone.0163360>
- [7] Fan, X., Zhou, Q., Liu, Z. and Xie, F. (2015) Electroencephalogram Assessment of Mental Fatigue in Visual Search. *Bio-Medical Materials and Engineering*, **26**, S1455-S1463. <https://doi.org/10.3233/BME-151444>
- [8] May, J.F. and Baldwin, C.L. (2009) Driver Fatigue: The Importance of Identifying Causal Factors of Fatigue when Considering Detection and Countermeasure Technologies. *Transportation Research Part F: Traffic Psychology and Behaviour*, **12**, 218-224. <https://doi.org/10.1016/j.trf.2008.11.005>
- [9] Utz, K.S., Hankeln, T.M.A., Jung, L., Lämmer, A., Waschbisch, A., Lee, De-Hyung, Linker, R.A. and Schenk, T. (2013) Visual Search as a Tool for a Quick and Reliable Assessment of Cognitive Functions in Patients with Multiple Sclerosis. *PLoS ONE*, **8**, e81531. <https://doi.org/10.1371/journal.pone.0081531>
- [10] Kitani, T., *et al.* (2011) Term Committee of Japanese Society of Fatigue Science. *Nihon Hirougakkaishi*, **6**, 1. (in Japanese)
- [11] Swets, J. (1988) Measuring the Accuracy of Diagnostic Systems. *Science*, **240**, 1285-1293. <https://doi.org/10.1126/science.3287615>

Novel Method Employing Accelerated-Oscillated Wave Saline Solutions to Unblock Blood Vessels—Physics and Fluid Dynamics Perspectives and Simulations

Stephon Stewart, Dineshen Chuckravanen*

British Association of Cognitive Neuroscience (BACN), Department of Psychology, University of Essex, Colchester, UK

Email: *dineshen2013@gmail.com

How to cite this paper: Stewart, S. and Chuckravanen, D. (2021) Novel Method Employing Accelerated-Oscillated Wave Saline Solutions to Unblock Blood Vessels—Physics and Fluid Dynamics Perspectives and Simulations. *Open Journal of Biophysics*, 11, 415-424.

<https://doi.org/10.4236/ojbiphy.2021.114018>

Received: August 17, 2021

Accepted: October 26, 2021

Published: October 29, 2021

Copyright © 2021 by author(s) and Scientific Research Publishing Inc.

This work is licensed under the Creative Commons Attribution International License (CC BY 4.0).

<http://creativecommons.org/licenses/by/4.0/>



Open Access

Abstract

This research assesses the speed of blood flow across blood vessels and more specifically the veins in terms of Reynold's number (laminar flow vs. turbulence flow) and in terms of overall speed of the blood when being injected with high-speed saline particles. The authors propose a novel technique to generate accelerated-waved particles built from saline solution to enable the unblocking of partially-blocked healthy-walled veins, and to restore normal operations of these veins. The novel technique encompasses a pump that accelerates saline solutions into the blood stream of the vein and these oscillated waves break down the fats or deposits inside the veins in order to help the blood to flow freely without any obstruction. This research simulated the vein with blood stream using characteristics of the vein in terms of vein diameter, blood density, venous blood flow, and the viscosity of the blood at the normal body temperature. The speed of the overall blood flow after the injection of the accelerated saline droplet solution was determined as well as the depth of penetration of the accelerated particles in order to cleanse the inside of the vein. Results are promising in terms of not altering significantly the overall speed of the bloodstream and also in terms of efficacy of the length of the vein which is being cleaned using this accelerated particle method.

Keywords

Arteries, Mathematical Models and Simulations, Sound-Waved Particle Fluids, Unblocking Blood Vessels, Veins

1. Introduction

The concept which is proposed here for the unblocking of blood vessels (such as

veins and arteries) that are hindered by fat deposits or small clots that are found inside the blood vessels is analogous to the working of sound waves in the inner ear. Sound-waved fluids or solutions with pH similar to blood or saline solution will be injected/cathetered into the bloodstream to create ripples or waves for unblocking blood vessels. Generally speaking, the normal saline solution is a mixture of water and salt and its salt concentration resembles that of tears, blood and other body fluids (0.9% saline) and it is also referred to as an isotonic solution. Therefore, a normal saline solution is considered soothing and friendly to the human body [1]. In order to explain the concept which is used in this research, we will explain in detail how the employed concept in this research mimics the concept of the working of the inner ear.

1.1. Concept Analogous to Working in Inner Ear

Hearing relies on a series of complicated stages that transform sound waves in the air into electrical signals. The auditory nerve transports these signals to the brain subsequently. The sound waves enter the outer ear and then travel along the ear canal leading to the eardrum. The latter then vibrates based on the sound waves that are incident on the eardrum and consequently send these vibrations to tiny bones in the middle ear that are the 1) malleus; 2) incus; and 3) stapes. These bones amplify the sound vibrations and then these are sent to the cochlea which is snail-shaped structure full with fluids in the inner ear. The vibrations cause the fluid inside the cochlea to ripple (vibrate) which produces a travelling wave along the basilar membrane. Hair cells that are found on top of the basilar membrane ride the wave. Sensory cells (hair cells) that are near the wide end of the cochlea detect high-frequency sounds and those that are closer to the center detect low-frequency sounds [2] [3] [4] [5].

Figure 1 demonstrates that the fluid in the top-most tube is set in motion by the application of the piston-like movements of the stapes on the oval window (Left of the figure). The vibrations travel into the fluid of the upper tube of the cochlea and around the tip of the organ into the fluid of the lower tube. One can clearly observe the ripple which is formed in this particular part of the cochlea region.

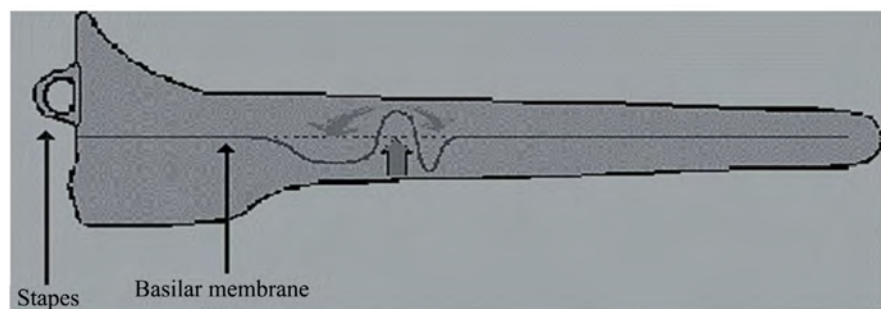


Figure 1. Ripple wave in the fluid of the upper tube of the cochlea owing to vibrations of sound waves.

Therefore, similar ripple like waves will be generated such that these waves are accelerated inside the blood vessels to unblock clots or fats stuck on the inner wall of the veins. Next, the general characteristics of the blood vessels are described.

1.2. General Characteristics of Blood Vessels

The arterial blood flow velocities are in the region of 4.9 to 19 cm/s while the venous blood flow ranges from 1.5 to 7.1 cm/s. The diameters of the blood vessels range from 800 μm to 1.8 mm. The blood flow rate in arteries ranges from 3.0 to 26 ml/minute while the blood flow rate in veins ranges from 1.2 to 4.8 ml/minute. The blood flow velocity is the fastest in the middle of the vessel and slowest at the vessel wall owing to friction. Moreover, as viscosity decreases, blood flow increases and so does an increase in perfusion. The resistance to blood flow is inversely proportional to the 4th power of the radius of the blood vessel.

2. Methodology

Before elaborating the simulation part, it is crucial to be aware of the following technical terms in terms of types of blood flow in the blood vessels.

2.1. Laminar Flow

Laminar flow is shown by the smooth streamlines (see **Figure 2**) and highly ordered motion and if the blood vessel is long as compared to the entry length then the entrance effects are negligible and the flow is fully developed. The laminar flow happens when the fluid flows in parallel layers without mixing. The velocity of the fluid is constant at any given moment. As the flow is constant, there is no acceleration. The flow is laminar for cylindrical pipes when the Reynolds number is about less than 2500.

2.2. Transition from Laminar Flow to Turbulent Flow

The change from laminar to turbulent flow is not too sudden, it normally occurs over a certain region in which the turbulent flow in the center of the blood vessel

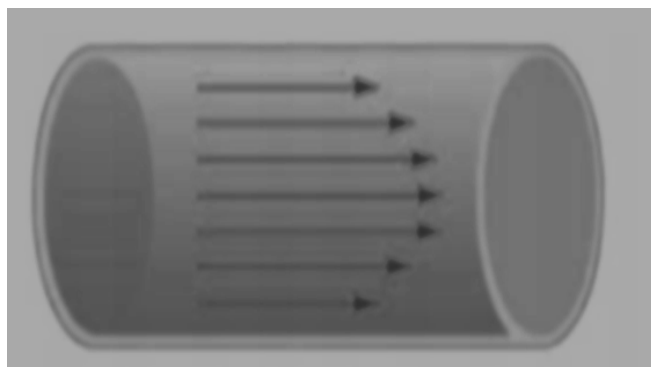


Figure 2. Laminar flow of blood stream in blood vessel.

and the laminar flow is near the edges of the pipe. The blood flow oscillates between laminar and turbulent flows before it becomes totally turbulent. The flow is transitional when the Reynolds number lies in-between 2300 and 4000.

Turbulent Flow in Blood Vessel

Turbulent flow occurs by velocity oscillations and highly disordered motion. Turbulent flow happens when streamlines of the liquid are irregular and change over time (see **Figure 3**). The path of the fluid flow is irregular and form tiny whirl-pool regions and the blood flow is turbulent when Reynolds number is greater than 4000. The Reynolds number can reveal whether flow is laminar or turbulent. The transition from laminar to turbulent flow depends on the surface roughness, flow velocity, geometry, surface temperature, and type of fluid.

The flow regime relies on the ratio of inertial forces to viscous forces in the fluid. This ratio is called the Reynolds number and is expressed as:

$Re = \text{Inertial Force} / \text{Viscous Force}$:

$$Re = \frac{\rho V_{avg} D}{\mu} = \frac{V_{avg} D}{\nu}$$

In this equation, ρ represents the density of the fluid (SI units: kg/m^3), V_{avg} represents the average flow speed (m/s), D is the diameter of the tube (m), μ represents the dynamic viscosity of the fluid (Pa-s or N-s/m² or kg/(m-s)) and ν denotes the kinematic viscosity of the fluid (m²/s). The critical Reynolds number Re is the number at which the flow becomes turbulent.

3. Experiments/Simulations

All simulations were conducted using Matlab software R2021 and a computer of the following properties (i7-7820HQ CPU @ 2.90 GHz and RAM memory 16 GB).

Simulation 1

The velocity profile of the bloodstream for a determined Reynold number is based on the average velocity of the blood flow in the vein (blood vessel). In order to do the simulation of the behavior of the vein, we have to consider the general characteristics of the vein for an adult (human). The following information relate to the specific features of the human vein and these are outlined as follows [6] [7] [8].



Figure 3. Turbulent flow of blood stream in blood vessel.

- Blood density = 1060 kg/m^3
- Vein's diameter = 2 cm (For instance, the average inferior vena cava diameter for an adult is around 2 cm (0.78 in))
- Venous blood flow = 7.0 cm/s
- Viscosity of blood = 4.0 cp (ranges from 3.5 to 5.5 cp for normal)
- At normal level, in pascal-second (Pa·s), the viscosity of blood at 37°C is normally 3×10^{-3} to 4×10^{-3} [8], respectively 3 to 4 centipoise (cP) in the centimetre gram second system of units.
- $\mu = (3 \text{ to } 4) \times 10^{-3} \text{ Pa}\cdot\text{s}$ ←
- $v = \mu/\rho = \{(3 \text{ to } 4) \times 10^{-3}/1.06 \times 10^3\} = (2.8 \text{ to } 3.8) \times 10^{-6} \text{ m}^2/\text{s}$ ←

The Reynold's number was determined by the Matlab software to be **397.5 Re** (see **Figure 4** and **Figure 5**) and it differs owing to speed of the blood flow and these depend on the chosen characteristics as mentioned before.

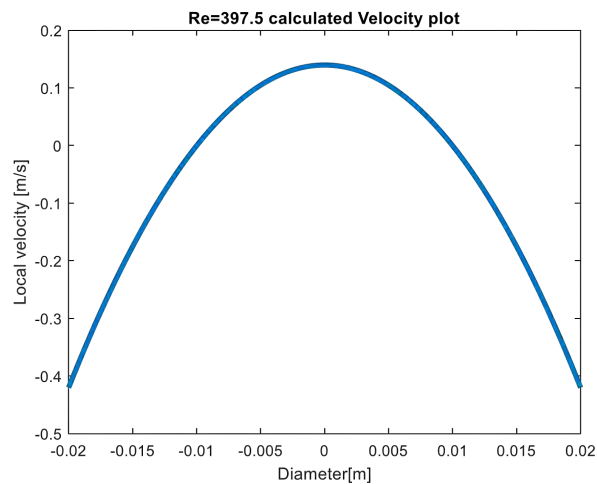


Figure 4. The velocity of the blood stream which is locally in the blood vessel with Reynold's number being 397.5.

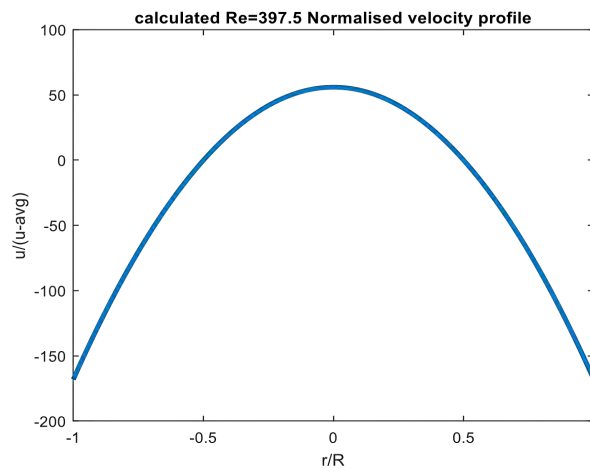
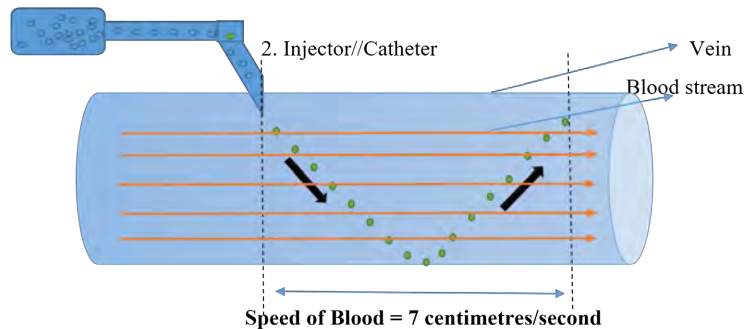


Figure 5. The normalized velocity profile of the blood stream across the blood vessel where R is the radius of the blood vessel and r is the distance from the mid-point of the blood vessel.

Simulation 2

For the second simulation, particle accelerated fluid by injection passes through the blood vessel (vein). The sketch below represents the oscillating pump which pumps the saline solution.



Let us assume that the blood flow is 7.0 cm per second in the vein, the diameter of the vein is 2 cm and the volume of blood flow per second is calculated using the volume of cylinder equation:

Step 1: Volume of blood flow per second

$$\text{Volume of cylinder} = \pi r^2 h$$

$$\text{Radius } (r) = 2/(2 \times 100) \text{ metres}$$

$$\text{Height } (h) = 7/100 \text{ metres}$$

$$\text{Volume of Cylinder} = \text{Volume of blood flow per second} = 2.1991 \times 10^{-5} \text{ m}^3$$

Step 2: Mass of blood per second

Using the density of blood, one can compute the mass of blood using the following equation:

Let the Mass of blood be M_b , the density of blood be ρ_b and the volume of blood be V_b .

$$\frac{\text{Mass of blood}}{\text{Volume of blood}} = \text{Density of blood}$$

Assuming that the density of blood is $1060 \text{ kg}\cdot\text{m}^{-3}$

$$M_b = \rho_b \times V_b$$

$$M_b = 1060 \times V_b$$

$$M_b = 1060 \times 2.1991 \times 10^{-5}$$

$$M_b = 0.0233 \text{ kg}$$

Step 3: Determine the number of oscillated fluid wave particles per centimeter

Let us assume that the shape of the accelerated particle is spherical and therefore the volume of sphere is $\frac{4\pi r^3}{3}$ [9].

Now let us use a syringe tip of 0.3 mm and therefore the particle emanated from this tip will have a maximum diameter of 0.3 mm.

Thus the volume of 1 particle-accelerated fluid:

$$\frac{4\pi(0.3/2000)^3}{3} = 1.4137 \times 10^{-11} \text{ m}^3 \leftarrow$$

Step 4: Using a pump frequency of 300 Hz to find mass of particles

In this case scenario, we will be using a pump frequency of 300 Hz (300 samples per second which insinuates that 300 accelerated particles of saline fluids will be injected per second in the vein and also the saline solution has the same density of blood which is 1060 kg/m^3 [10].

Mass of injected particles (M_p) = Total Volume of particles (per centimetre) \times Density of the particle

$$M_p = \text{Number of particles injected per centimetre} \times 1060$$

$$M_p = 300 \times 1.4137 \times 10^{-11} \times 1060$$

$$M_p = 4.4956 \times 10^{-6} \text{ kg} \leftarrow$$

Step 5: Conservation of momentum to determine overall speed of the blood stream bombarded with the accelerated particle fluids [11]

$$M_b V_b + M_p V_p = M_{\text{total}} * V_{\text{average}}$$

$$V_{\text{average}} = \left((0.0233 \times 7.0 \text{ cm/s}) + (4.4956 \times 10^{-6} \times 300) \right) / (0.0233 + 4.4956 \times 10^{-6})$$

$$V_{\text{average}} = 7.0565 \text{ cm/s}$$

Therefore, the speed of the total mass of blood and the accelerated particles of saline solution is 7.0565 cm/s .

Now, the next last step is to find how far this saline-blood stream will move across the vein until it reaches again its original blood stream of 7.0 cm/s so that one can quantify the life span of the particles in performing their duties of de-blocking partially blocked veins. In order to determine this, we will resort to kinematic motion.

Step 6: Use of kinematic motion to find how far these accelerated particles can maintain this speed (Step 5)

Using the famous equation of $V^2 = U^2 + 2as$ where V is the final velocity of an object, U is the initial velocity of an object, a is the acceleration of the object and s is the displacement and we need to find a value for displacement s in metres [12].

$$\text{Displacement } (s) = (V^2 - U^2) / 2a = (7.0565^2 - 7.0^2) / 2a$$

$$\text{Acceleration } (a) = (V_2 - V_1) / \text{time} = (7.0565 - 7) / (1 \text{ second}) = 0.0565 \text{ cm/s}^2$$

$$\text{Displacement } (s) = (7.0565^2 - 7.0^2) / 2 \times 0.0565 = 7.0283 \text{ cm}$$

So this means that the accelerated fluid particles can perform the un-blocking task for a distance of about 7.03 cm .

Simulation: Varying the pump frequency and its effect of the depth of penetration of the accelerated particle saline solution

Figure 6 shows that when the pump frequency is increased, so does the penetration depth of the accelerated particles into the blood vessels but care should

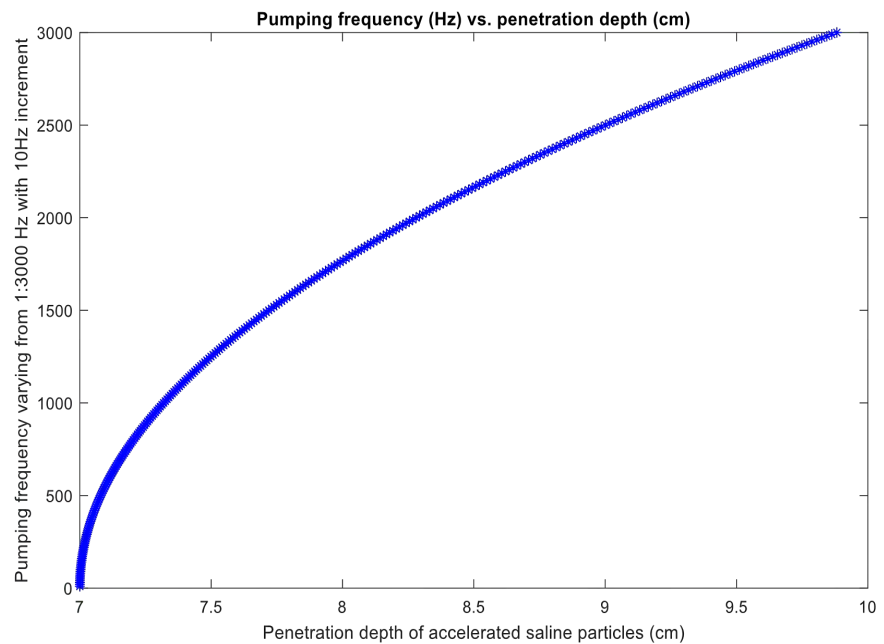


Figure 6. Curve produced while varying the pump frequency the penetration depth of the high speed particled solutions before reaching the original blood stream speed again.

be taken not to harm or break the blood vessels at such higher speeds and therefore speeds around 7cm/s seems safe as it is the original speed of the blood. For example, in order to reach a penetration depth of 7.5 cm, a 1200 Hz pump is required and higher frequency pump is more expensive to build and for the prototype, we envisage to build a pump with low frequency of 300 Hz and investigate what happen in ongoing works.

4. Discussions and Conclusions

This is a preliminary and novel method investigating how accelerated particle saline solutions can be used to un-block partially blocked blood vessels. This method involves only a small invasive part in order to insert the needle (Figure A1) at the localized position ideally some centimetres away from the blockages or fat deposits in order for the accelerated particle solution can cleanse the walls and remove debris or fat deposits or blockages of the blood vessels (such as the veins). The proposed novel method so far based on a thorough research in this field employed the biological process which is involved in the inner ear which is the rippled movement of fluid that is created when one hears a sound in the ear. The rippled fluid movement is used to cleanse the vein, artery or blood vessel. The frequency of the pump is crucial in the depth of penetration of the accelerated fluid particles in cleaning the inner walls of the blood vessels. Results from this novel method are promising in terms of safe use of this catheter medical technique and in terms of the overall speed of blood flow even being bombarded by high-speed fluid particles that are governed by the pump frequency.

Now, in the near future, we will improve the model in terms of the texture and

viscosity and ions actions that the saline solution can bring to this model in order to make it more efficient in curing blockages in the blood vessels (whether its arteries or veins). In order to achieve this, we will set up a physics laboratory where we will implement this novel method involving scientists, physicists and medical doctors.

Conflicts of Interest

The authors declare no conflicts of interest regarding the publication of this paper.

References

- [1] Tan, T.S., Tan, K.H., Ng, H.P. and Loh, M.W. (2002) The Effects of Hypertonic Saline Solution (7.5%) on Coagulation and Fibrinolysis: An *In Vitro* Assessment Using Thromboelastography. *Anaesthesia*, **57**, 644-648. <https://doi.org/10.1046/j.1365-2044.2002.02603.x>
- [2] Bellamy, M.L. and Frame, K. (Eds.) (1996) Neuroscience Laboratory and Classroom Activities. National Association of Biology Teachers and the Society for Neuroscience, 21-35.
- [3] Camhi, J.M. (1984) Neuroethology: Nerve Cells and the Natural Behavior of Animals. Sinauer Associates, Inc., Sunderland.
- [4] Kandel, E.R., Schwartz, J.H., and Jessell, T.M. (Eds.) (2000) Principles of Neural Science. 4th Edition, McGraw Hill Health Professions Division, New York.
- [5] Shepherd, G.M. (1994) Neurobiology. 3rd Edition, Oxford University Press, Oxford, New York.
- [6] Blood Flow, Blood Pressure, and Resistance. <https://courses.lumenlearning.com/nemcc-ap/chapter/blood-flow-blood-pressure-and-resistance/>
- [7] Yamazaki, M., Kusano, K., Ishibashi, T., Kiuchi, M. and Koyama, K. (2015) Intravenous Infusion of H₂-Saline Suppresses Oxidative Stress and Elevates Antioxidant Potential in Thoroughbred Horses after Racing Exercise. *Scientific Reports*, Article No. 15514. <https://doi.org/10.1038/srep15514>
- [8] Chaui-Berlinck, J.G., Monteiro, L.H., Navas, C.A. and Bicudo, J.E. (2002) Temperature Effects on Energy Metabolism: A Dynamic System Analysis. *Proceedings of the Royal Society Biological Science*, **269**, 15-19. <https://doi.org/10.1098/rspb.2001.1845>
- [9] Primitives—Blender Manual. <https://docs.blender.org/manual/en/latest/modeling/meshes/primitives.html>
- [10] Heinisch, M. (2015) Mechanical Resonators for Liquid Viscosity and Mass Density Sensing.
- [11] Britannica, T. (Ed.) (2021) Conservation of Momentum. Encyclopedia Britannica. <https://www.britannica.com/science/conservation-of-momentum>
- [12] Kleppner, D. and Kolenkow, R.J. (2010) An Introduction to Mechanics. Cambridge University Press, Cambridge, 112. <https://doi.org/10.1017/CBO9780511794780>

Appendix

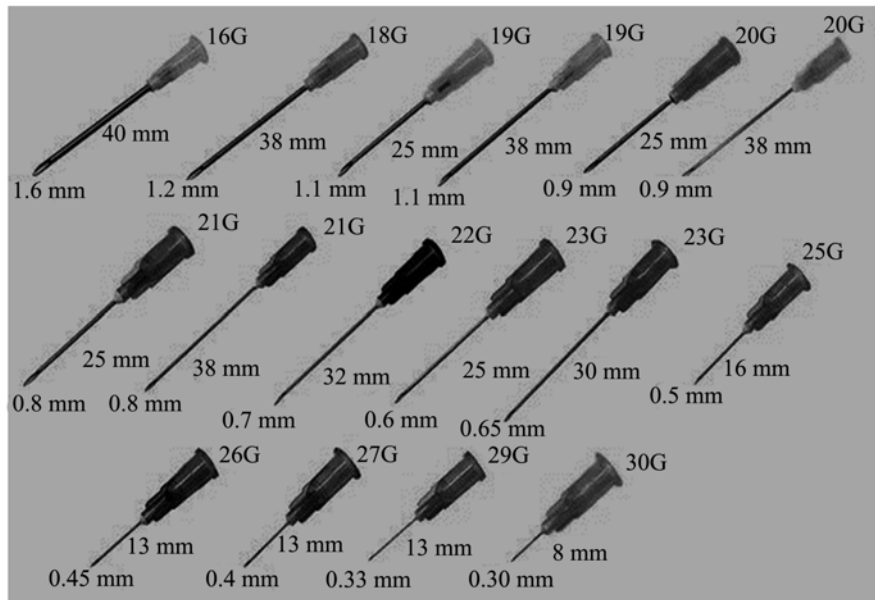
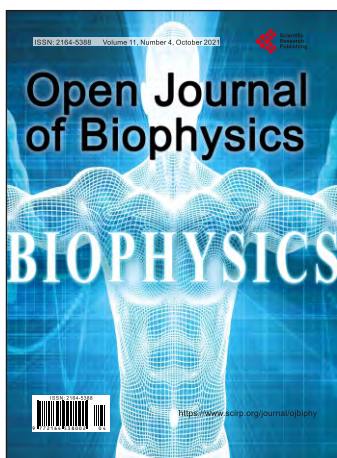


Figure A1. Types of needles and tips to demonstrate the one which is selected.



Call for Papers

Open Journal of Biophysics

ISSN Print: 2164-5388 ISSN Online: 2164-5396

<https://www.scirp.org/journal/ojbiphy>

Open Journal of Biophysics (OJBIPHY) is an international journal dedicated to the latest advancement of biophysics. The goal of this journal is to provide a platform for scientists and academicians all over the world to promote, share, and discuss various new issues and developments in different areas of biophysics.

Subject Coverage

All manuscripts must be prepared in English, and are subject to a rigorous and fair peer-review process. Accepted papers will immediately appear online followed by printed hard copy. The journal publishes original papers including but not limited to the following fields:

- Bioelectromagnetics
- Bioenergetics
- Bioinformatics and Computational Biophysics
- Biological Imaging
- Biomedical Imaging and Bioengineering
- Biophysics of Disease
- Biophysics of Photosynthesis
- Cardiovascular Biophysics
- Cell Biophysics
- Medical Biophysics
- Membrane Biophysics
- Molecular Biophysics and Structural Biology
- Physical Methods
- Physiology and Biophysics of the Inner Ear
- Proteins and Nucleic Acids Biophysics
- Radiobiology
- Receptors and Ionic Channels Biophysics
- Sensory Biophysics and Neurophysiology
- Systems Biophysics
- Theoretical and Mathematical Biophysics

We are also interested in: 1) Short Reports—2-5 page papers where an author can either present an idea with theoretical background but has not yet completed the research needed for a complete paper or preliminary data; 2) Book Reviews—Comments and critiques.

Notes for Intending Authors

Submitted papers should not have been previously published nor be currently under consideration for publication elsewhere. Paper submission will be handled electronically through the website. All papers are refereed through a peer review process. For more details about the submissions, please access the website.

Website and E-Mail

<https://www.scirp.org/journal/ojbiphy>

E-mail: ojbiphy@scirp.org

What is SCIRP?

Scientific Research Publishing (SCIRP) is one of the largest Open Access journal publishers. It is currently publishing more than 200 open access, online, peer-reviewed journals covering a wide range of academic disciplines. SCIRP serves the worldwide academic communities and contributes to the progress and application of science with its publication.

What is Open Access?

All original research papers published by SCIRP are made freely and permanently accessible online immediately upon publication. To be able to provide open access journals, SCIRP defrays operation costs from authors and subscription charges only for its printed version. Open access publishing allows an immediate, worldwide, barrier-free, open access to the full text of research papers, which is in the best interests of the scientific community.

- High visibility for maximum global exposure with open access publishing model
- Rigorous peer review of research papers
- Prompt faster publication with less cost
- Guaranteed targeted, multidisciplinary audience



**Scientific
Research
Publishing**

Website: <https://www.scirp.org>

Subscription: sub@scirp.org

Advertisement: service@scirp.org